



ELSEVIER

Tectonophysics 318 (2000) 119–159

**TECTONOPHYSICS**

www.elsevier.com/locate/tecto

# Motion of the Rivera plate since 10 Ma relative to the Pacific and North American plates and the mantle

Charles DeMets \*, Stephen Traylen

*Department of Geology and Geophysics, University of Wisconsin-Madison, 1215 West Dayton Street, Madison, WI 53706, USA*

Received 4 January 1999; accepted for publication 30 August 1999

---

## Abstract

To better understand the influence of Rivera plate kinematics on the geodynamic evolution of western Mexico, we use more than 1400 crossings of seafloor spreading magnetic lineations along the Pacific–Rivera rise and northern Mathematician ridge to solve for rotations of the Rivera plate relative to the underlying mantle and the Pacific and North American plates at 14 times since 9.9 Ma. Our comparison of magnetic anomaly crossings from the undeformed Pacific plate to their counterparts on the Rivera plate indicates that significant areas of the Rivera plate have deformed since 9.9 Ma. Dextral shear along the southern edge of the plate from 3.3–2.2 Ma during a regional plate boundary reorganization deformed the Rivera plate farther into its interior than previously recognized. In addition, seafloor located north of two rupture zones within the Rivera plate sutured to North America after 1.5 Ma. Anomaly crossings from these two deformed regions thus cannot be used to reconstruct motion of the Rivera plate. Finite rotations that best reconstruct Pacific plate anomaly crossings onto their undeformed counterparts on the Rivera plate yield stage spreading rates that decrease gradually by 10% between 10 and 3.6 Ma, decrease rapidly by 20% after 3.6 Ma, and recover after 1 Ma. The slowdown in Pacific–Rivera seafloor spreading at  $\sim 3.6$  Ma coincided with the onset of dextral shear across the then-incipient southern boundary of the Rivera plate with the Pacific plate. The available evidence indicates that the Rivera plate has been an independent microplate since at least 10 Ma, contrary to published assertions that it fragmented from the Cocos plate at  $\sim 5$  Ma. Motion of the Rivera plate relative to North America has changed significantly since 10 Ma, in concert with significant changes in Pacific–Rivera motion. A significant and robust feature of Rivera–North America motion not previously recognized is the cessation of margin-normal convergence and thus subduction from 2.6 to 1.0 Ma along the entire plate boundary, followed by a resumption of trench-normal subduction along the southern half of the Rivera–North America plate boundary after 1.0 Ma. Motion of the Rivera plate relative to the underlying mantle since 10 Ma has oscillated between periods of landward motion and seaward motion. The evidence suggests that the torque exerted by slab pull on this young and hot oceanic plate is either minimal or is effectively counterbalanced by forces that resist its motion. © 2000 Elsevier Science B.V. All rights reserved.

*Keywords:* geodynamics; Jalisco block; Mathematician plate; microplate; Rivera plate

---

\* Corresponding author. Fax: +1-608-262-0693.

*E-mail address:* chuck@geology.wisc.edu (C. DeMets)

## 1. Introduction

The collision of the Pacific–Farallon seafloor spreading center with the western convergent margin of North America at ~28 Ma marked the beginning of a profound change in the tectonic and volcanic evolution of western North America (Atwater, 1970, 1989). As the spreading segments and transform faults of the Pacific–Farallon rise approached and collided with the North American continental margin, the Farallon plate gradually fragmented into a series of smaller plates. Some of these small plates eventually sutured to the Pacific plate west of peninsular California (Lonsdale, 1991). Others are still subducting beneath North America. The well-surveyed pattern of seafloor magnetic lineations produced by spreading along the western boundaries of these microplates has been used to construct detailed kinematic models of the motions of the Farallon fragments relative to the neighboring Pacific and North American plates (e.g. Atwater, 1970; Engebretson et al., 1985; Stock and Molnar, 1988; Lonsdale, 1989; Fernandez and Hey, 1991; Wilson, 1993a). These models have in turn become important elements in our understanding of the tectonics of western North America (Atwater, 1970; Lipman, 1980; Atwater, 1989; Stock and Hodges, 1989; Nicholson et al., 1994; Stock and Lee, 1994; Bohannon and Parsons, 1995).

The Rivera plate, the smallest remaining active fragment of the Farallon plate, presently subducts beneath North America at the northern end of the Middle America trench and accretes seafloor along its western boundary, the Pacific–Rivera rise (Fig. 1). The well-surveyed and easily deciphered seafloor spreading magnetic lineations created along the Pacific–Rivera rise provide the basis for reconstructing the motion of the Rivera plate relative to the Pacific plate and via local and global plate circuit closures, relative to the adjacent North American and Cocos plates. Numerous studies have already used the seafloor spreading lineations younger than 4 Ma to solve for rotations that describe present-day Pacific–Rivera plate motion (Klitgord and Mammerickx, 1982; Lonsdale, 1989; DeMets and Stein, 1990; Lonsdale, 1991; Bandy, 1992; Bandy and Pardo, 1994; Lonsdale, 1995;

DeMets and Wilson, 1997). As a consequence, our understanding of the present motion of the Rivera plate relative to neighboring plates is excellent, although not without controversy (Bandy et al., 1998; Wilson and DeMets, 1998). Studies of Pacific–Rivera kinematics for times older than ~4 Ma (Lonsdale, 1989, 1991, 1995) have additionally defined important aspects of the geometric evolution of the Rivera plate and its boundaries.

Surprisingly, no study has applied standard plate reconstruction techniques to the entire 10 Ma record of Pacific–Rivera seafloor spreading, despite the potential utility of such a model for studies of deformation and volcanism within the Jalisco region of western Mexico (Fig. 1). For example, workers investigating: (1) arc-normal extension in the past 5 Ma across the Colima graben and Manzanillo trough (e.g. Nixon, 1982; Luhr et al., 1985; Bourgeois et al., 1988; DeMets and Stein, 1990; Johnson and Harrison, 1990; Bandy and Pardo, 1994; Stock and Lee, 1994; Bandy et al., 1995; Kostoglodov and Bandy, 1995); (2) transtensional faulting along the Tepic–Zacoalco fault zone (Fig. 1) (Ferrari et al., 1994; Richter et al., 1995); and (3) diverse and unusual volcanism from stratovolcanos and within grabens in the Jalisco block (Lange and Carmichael, 1991; Wallace et al., 1992; Delgado Granados, 1993) all postulate that these phenomena are related to subduction of the Rivera plate beneath North America.

An important motivation for this work is to satisfy the need for more detailed information about the post-10 Ma history of Rivera plate motion relative to North America. In this paper, we apply well-accepted quantitative techniques to the entire 10 Ma seafloor spreading record of the Pacific–Rivera rise. Our work complements previous studies of Rivera plate motion prior to 4 Ma in the following respects:

(1) We describe the underlying reconstruction techniques and present the model rotations and uncertainties.

(2) We present evidence for distributed deformation that extends farther north into the Rivera plate than previously thought, and we describe constraints on the timing of that deformation.

(3) We solve for the motion and stage velocities

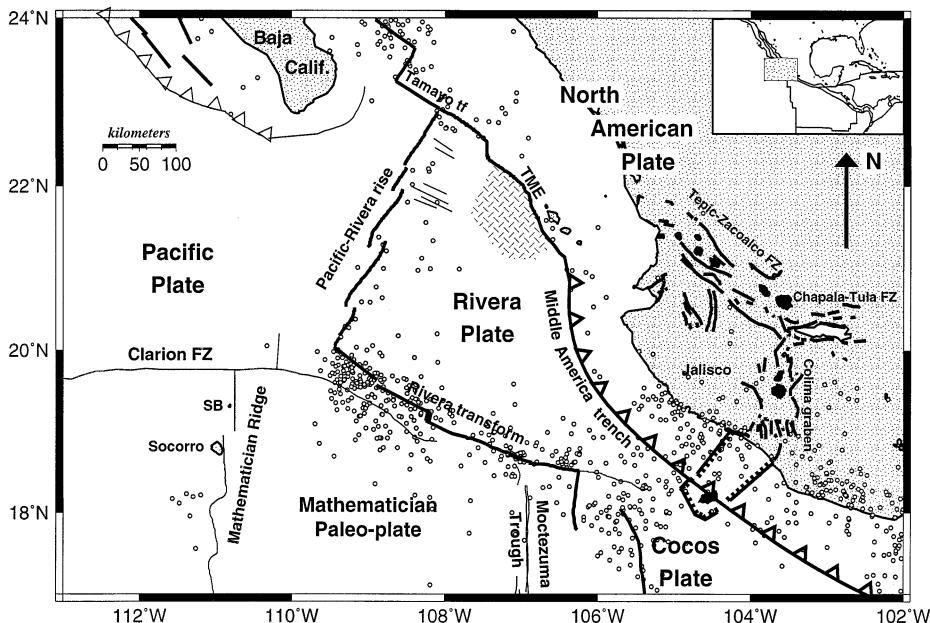


Fig. 1. Location map for post-10 Ma tectonic features in the Rivera plate region. The Clarion fracture zone is defined from seafloor bathymetry and is named following Lonsdale (1995); this feature was designated the San Benedicto fracture zone by Lonsdale (1991). Bold and thin lines represent active and inactive faults, respectively. Black areas show locations of major Quaternary volcanism. Open circles show 1967–1999 teleseismically located earthquakes shallower than 60 km. The hatched area designates seafloor created along the Maria Magdalena rise and may contain continental remnants from the opening of the Gulf of California (Lonsdale, 1995). SB: San Benedicto island; TME: Tres Marias Escarpment.

for the Rivera plate relative to North America and the mantle using rotations that describe motion of the Pacific plate relative to North America (Atwater and Stock, 1998; DeMets and Dixon, 1999) and the hotspots (Gripp and Gordon, 1990).

(4) We solve for the post-10 Ma spreading history of the northern Mathematician ridge, primarily to demonstrate that the Rivera plate has moved independently from neighboring oceanic plates since at least 10 Ma.

To achieve these objectives, we first describe the magnetic anomaly crossings and conjugate points that we use, their uncertainties, and the techniques that we employ. We then solve for the nature and timing of Rivera plate deformation by comparing the geometries of the paleo-spreading centers preserved on the presumably undeformed Pacific plate to their counterparts on the Rivera plate. Using the subset of magnetic anomaly crossings that record motion of the undeformed parts of the Rivera plate, we solve for Pacific–Rivera finite

rotations and stage velocities, and we present reconstructions for these two plates as well as the North American and Mathematician plates. We then solve for the motion of the Rivera plate relative to North America and the underlying mantle, and conclude by discussing the implications of our new model and plate reconstructions for the tectonic evolution of the Jalisco region of western Mexico since 10 Ma and the dynamics of the Rivera plate.

## 2. Methods

### 2.1. Solving for best-fitting rotations

Finite rotations and their covariances are derived using a general method for finding the rotation that best reconstructs ship-board and airplane crossings of magnetic anomalies and frac-

ture zones that define a paleo-seafloor spreading center (Hellinger, 1979; Chang, 1988). Crossings of magnetic anomalies are first grouped into a series of paleospreading segments and are assigned to a fixed or a moving plate. The best-fitting rotation is then defined as the rotation that minimizes the least-squares scatter ( $\chi^2$ ) of the fixed and rotated crossing points from the great circle segments that best fit those points. Three adjustable parameters are required to fully characterize the rotation that reconstructs the data, and two parameters are required to describe each of the  $S$  great circle segments that best fit groups of reconstructed anomaly crossings. Optimizing the fit thus requires adjustment of  $2S+3$  parameters. Descriptions of the techniques and the derivation of statistically rigorous rotation covariances are given by Hellinger (1979, 1981), Chang (1988), and Royer and Chang (1991).

Information regarding finite opening directions is normally supplied by fracture zones; however, no suitable transform faults have offset the Pacific–Rivera rise since at least 10 Ma. We thus assume that paleo-slip directions have been perpendicular to the paleo-rise axes and enforce this assumption by fitting conjugate points, which are features that by definition lie equidistant from the best-fitting finite rotation axis (Wilson, 1993a). The misfit of a trial rotation to a given conjugate pair is computed by rotating the conjugate point from the moving plate onto its fixed-plate counterpart, computing their respective angular distances to the trial pole of rotation, and then squaring the difference between these two angles while dividing by their combined uncertainties. Each pair of conjugate points adds one degree of freedom to the solution for a rotation, corresponding to this angular difference. Conjugate point misfits are measured in a direction orthogonal to misfits for reconstructed anomaly crossings, which means that conjugate points and anomaly crossings impose geometrically independent constraints on best-fitting rotations and their uncertainties. Conjugate points determine the great circle along which the best-fitting rotation lies and magnetic anomaly crossings determine both the distance to the best-fitting pole and the total opening angle. Similarly, uncertainties in conjugate point locations, when propagated into the covariances that describe rota-

tion uncertainties, constrain the component of the covariances that describes the uncertainty in the location of a reconstructed point in a direction that parallels seafloor spreading lineations.

## 2.2. Determining optimal paleo-rise segmentations

For regions of the seafloor lacking detailed bathymetry, paleo-axial discontinuities such as overlapping spreading segments or higher-order ridge-axis discontinuities (Macdonald et al., 1991) can be difficult to detect because the 10 km-or-less offsets typical of such discontinuities tend to be masked by the random scatter typical of magnetic anomaly crossings. To solve for the simplest paleo-axial geometry that is consistent with magnetic anomaly crossings of a given age, we implement a simple iterative search for a segment boundary in a manner analogous to the search for an additional plate boundary described by Stein and Gordon (1984). Given a group of magnetic anomaly crossings,  $\chi^2$  is determined for the great circle that simultaneously best fits all of the crossings. The same anomaly crossings are then divided into two subsets at an intermediate point, and the values of  $\chi^2$  for the great circles that best fit the respective subsets of the anomaly crossings are determined. The latter procedure is repeated at many different intermediate locations along the paleo-spreading center to determine how the fit of the two-segment models changes as a function of distance along the paleo-spreading center. For the two-segment model that provides the best overall fit, the significance in the improvement of the fit relative to that of a one-segment model is determined using an  $F$ -ratio test for two additional terms. Numerical experiments with synthetic data that simulate the characteristics of the data we employ indicate that this technique works well and is capable of distinguishing offsets greater than  $\sim 4$ –5 km.

## 3. Data

### 3.1. Magnetic anomaly crossings

To map seafloor spreading magnetic lineations along the Pacific–Rivera rise, we examined all non-proprietary ship-board magnetic and aeromagnetic

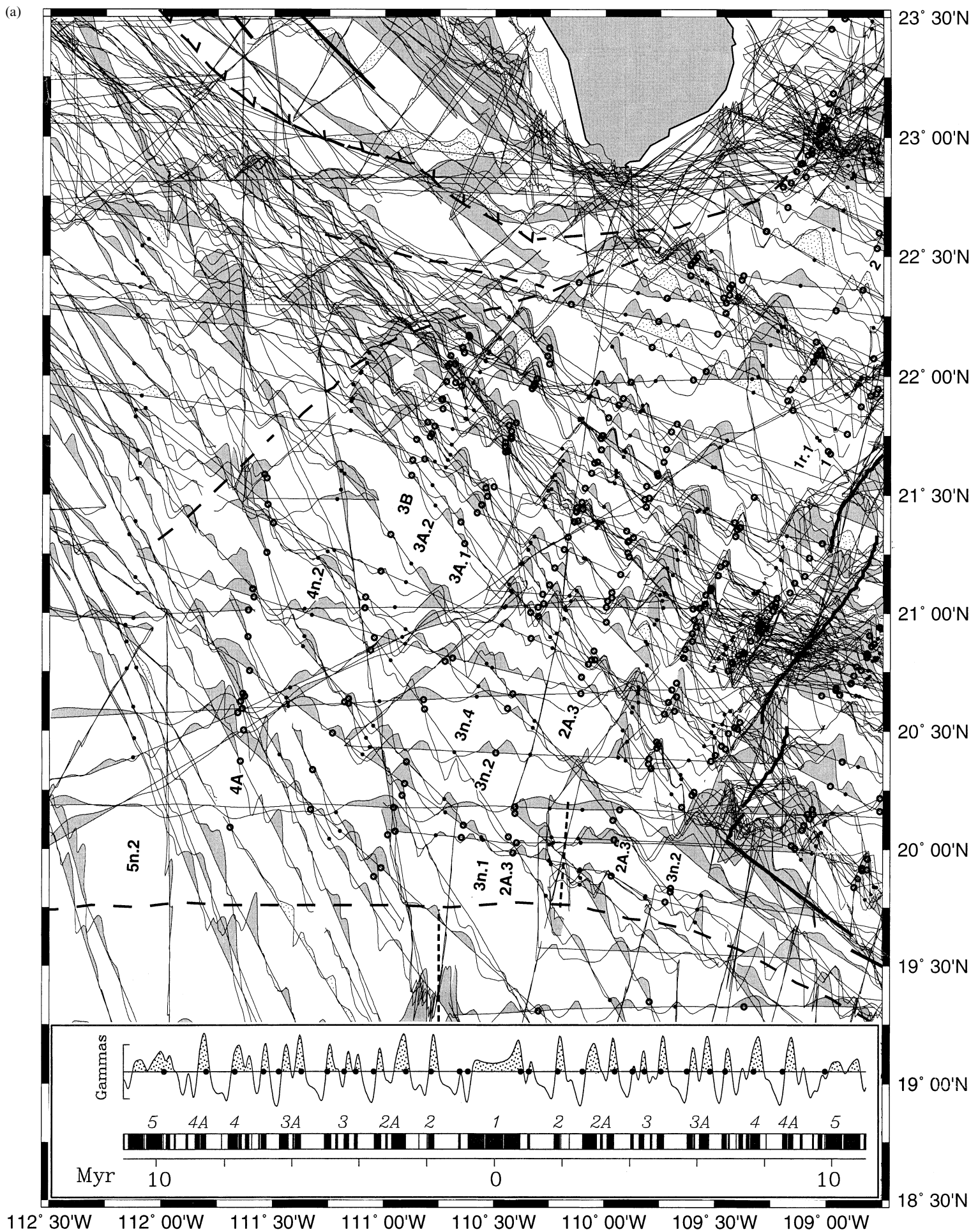


Fig. 2. Residual magnetic anomalies used in this study. All anomalies are projected onto N10°E. (a) Solid and open circles show crossings of the anomalies listed in Tables 2 and 3 and for clarity are alternated for adjacent anomalies. Tracks with more lightly shaded anomalies represent cruises with systematic navigational errors along some parts of the cruise track — these were downweighted in our inversions. Active and inactive tectonic boundaries are shown with solid and dashed lines, respectively. The inset shows a synthetic magnetic anomaly profile computed for a spreading azimuth of N70°W, ambient and remanent declinations and inclinations appropriate for this study area, and a constant full spreading rate of 60 mm/yr. Dots on the synthetic magnetic profile correspond to the ages for which we derived reconstructions (Table 2).

(b)

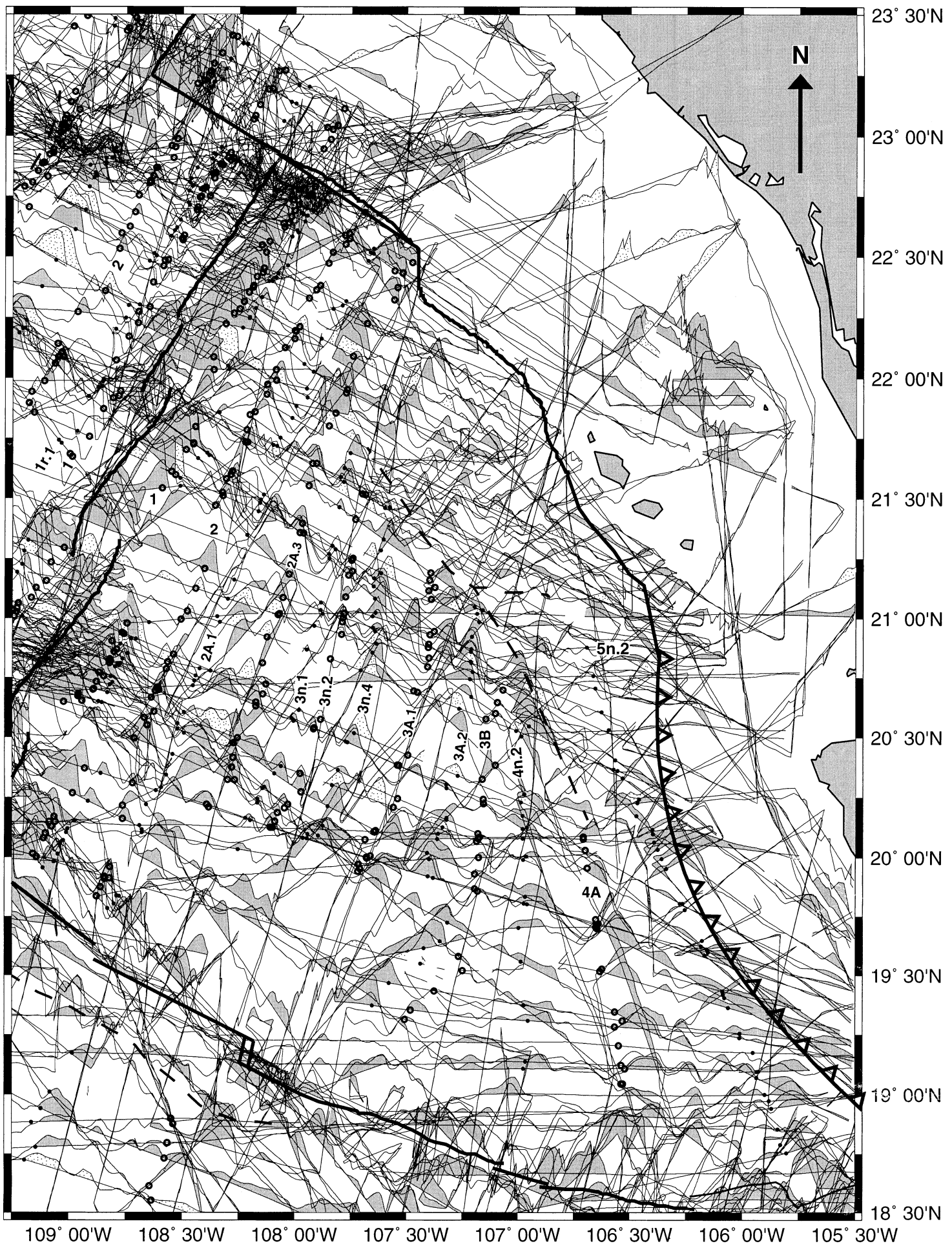


Fig. 2. (b) The figure is drawn to same scale as (a) and can thus be joined with it to construct a complete map of the Rivera plate magnetic anomaly data we used.

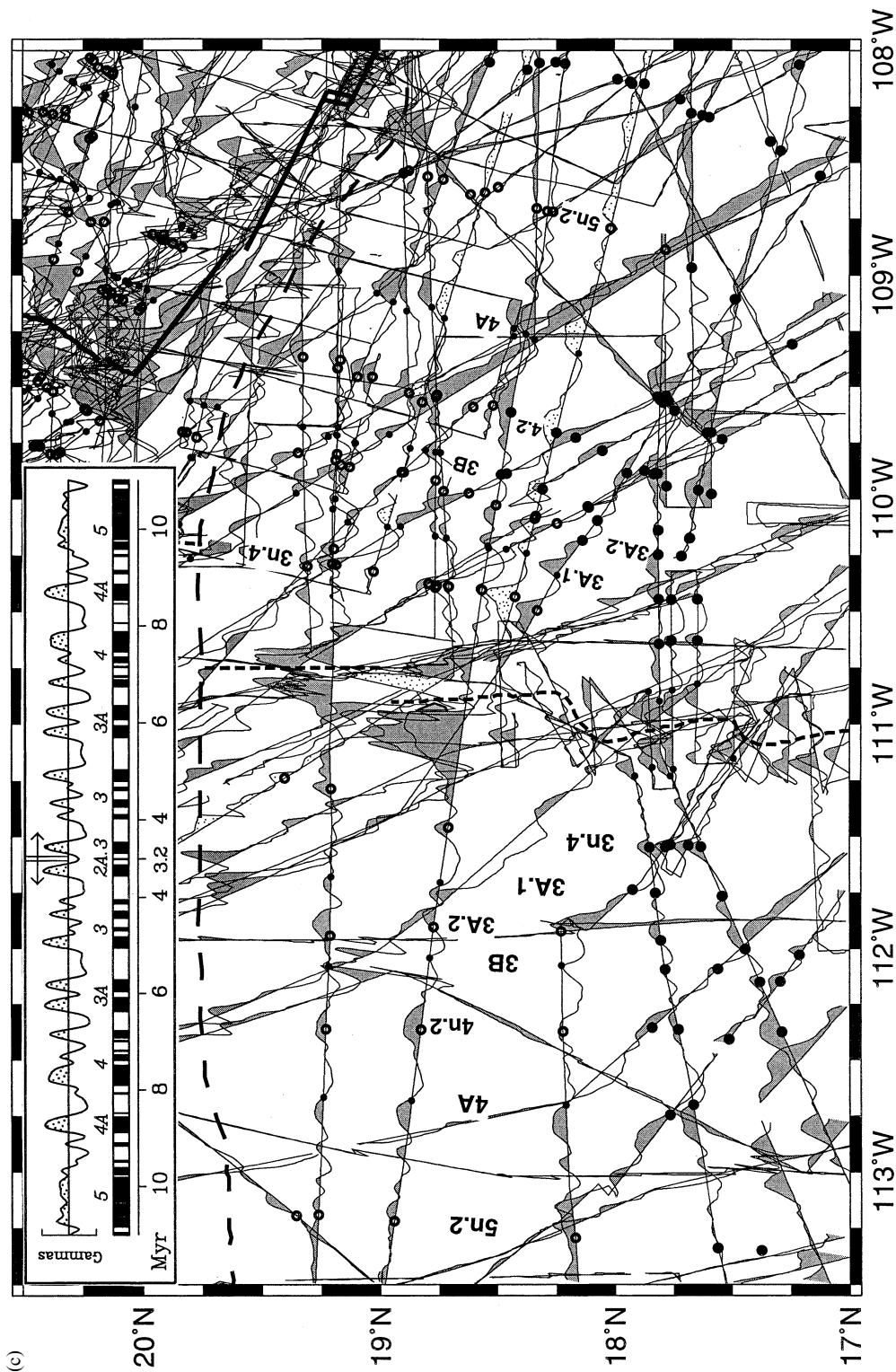


Fig. 2 (c) Magnetic anomalies along the Mathematician ridge north of 17°N. The synthetic profile shown in the inset was computed in a manner similar to the synthetic profile in (a), but assumes an east–west spreading azimuth and full spreading rate of 70 mm/yr.

Table 1

Cruises and flights that cross seafloor spreading lineations created at Pacific–Rivera rise and Mathematician ridge

Name	Name	Name	Name
0480-070 <sup>a</sup> (B)	DSDP 54	Hypo 01 (B)	Raitt 01 (A)
0480-305 <sup>a</sup> (B)	DSDP 63 (B)	Iguana 01 (B)	Raitt 03 (A)
0480-346 <sup>a</sup> (B)	DSDP 64 (B)	Iguana 05 (B)	Risethree 03 (B)
Aftermath 01 (B)	DSDP 65 (B)	<i>K. Keoki</i> 7401 (B)	SI 933 (B)
Ariadne 03 (A)	Deepsonde 02 (B)	<i>K. Keoki</i> 7812-2 (B)	Scan 11 (C)
Baja 75 <sup>b</sup> (C)	Doldrums 01 (C)	<i>K. Keoki</i> 7812-3 (B)	Siquieros 01 (B)
Baja 76A <sup>b</sup> (C)	Doldrums 02 (C)	Magma 01 (A)	<i>Thompson</i> 99 (B)
Baja 76B <sup>b</sup> (C)	Dolphin 02 (C)	Marsur 77 (B)	Tortuga 01 (A)
Benthiface 01 (B)	Drake 7501 (B)	Marsur 78 (C)	Tortuga 03 (A)
Carrousel 02 (C)	Drake 7505 (B)	<i>Moana Wave</i> 8705 (A)	<i>U. Maru</i> 03 (C)
Center 01 (B)	Drake 7701 (B)	ODP 138 (A)	Venture 03 (A)
Ceres 02 (B)	Drake 7706 (B)	ODP 140 (A)	<i>Vema</i> 2810 (B)
Ceres 04 (A)	Drake 7707 (B)	Oc-Coco (C)	<i>Washington</i> 65-1 (C)
<i>Charcot</i> 86003 (A)	Explorer 60 (C)	Papagayo 03 (C)	Wel 75 (B)
<i>Charcot</i> 87001 (B)	Gam 01 <sup>c</sup> (C)	Papatua 02 (A)	<i>Yaquina</i> 69 (C)
<i>Charcot</i> 87002	Gam 02 <sup>c</sup> (C)	Pascau 01 (A)	<i>Yaquina</i> 7102 (B)
Cocotow 01 (B)	Gambul 01 (C)	Phoenix 03 (A)	<i>Yaquina</i> 7110 (B)
Cocotow 04 (B)	Gambul 02 (C)	Pleiades 01 (B)	<i>Yaquina</i> 7302 (B)
<i>Conrad</i> 1005 (C)	Golfo 81 (A)	Plume 01 (A)	<i>Yaquina</i> 7309 (B)
<i>Conrad</i> 1203 (C)	Guaymas 01 (B)	Pol 6725 (C)	
Crisscross 03 (C)	Guaymas 03 (B)	Quebrada 02 (C)	

The letters A–C in parentheses designate the uncertainty category that applies to most crossings for a particular cruise (see text).

<sup>a</sup> Project Magnet flight; National Geophysical Data Center designator.

<sup>b</sup> Some anomaly crossings were eliminated due to significant systematic navigational offsets from nearby cruises.

data archived at the Lamont-Doherty Earth Observatory, the National Geophysical Data Center, and Scripps Institution of Oceanography as of April 1996 (Fig. 2a–c and Table 1). We limited our analysis primarily to magnetic anomalies younger than or equal in age to anomaly 5n.2, which is the oldest correlatable magnetic anomaly on the Rivera plate (Figs. 2 and 3). We further limited ourselves to magnetic anomalies located south of the prominent conjugate pseudo-faults that are located northwest and east of the present rise axis (Fig. 3).

Our magnetic anomaly correlations (Fig. 2a–c) are similar to older interpretations of subsets of these data (Klitgord and Mammerickx, 1982; Lonsdale, 1989) and are the same as a recent interpretation of magnetic data from the same region (Lonsdale, 1995). To establish the basis for detailed reconstructions of the Rivera plate since anomaly 5n.2, we used an interactive display of the digital anomaly profiles to extract the coordinates of each ship or airplane crossing of 14 points

on the magnetic reversal time scale ranging from anomaly 1 (0.78 Ma) to the young edge of anomaly 5n.2 (9.92 Ma). We eliminated some or all data from several older cruises that lacked satellite navigation and were clearly affected by systematic navigational error (e.g. Gam-2, Baja 75, Baja 76). Navigation for the Marsur 78 cruise also appeared to be less reliable than for other cruises from the 1970s, leading us to downweight all anomaly crossings from this cruise. We also downweighted or eliminated anomaly crossings near or over seamounts and occasionally adjusted uncertainties for individual anomaly crossings up or down one category for well expressed or poorly expressed anomalies. Ultimately, we identified over 1100 magnetic anomaly crossings from 82 cruises and aeromagnetic flights in this region (Table 1).

We also analyzed magnetic anomalies from cruises traversing the northernmost segments of the Mathematician ridge (Figs. 2c and 3). We restricted this part of the analysis to anomaly crossings located north of  $\sim 18^\circ\text{N}$ ; these appear



To determine the dispersions of the anomaly crossings in each of three categories, we constructed data sets that consisted only of Category A, B, or C anomaly crossings for each of the 14 times modeled. We then derived best-fitting rotations for each set of data and determined the distances of the reconstructed anomaly crossings from their best-fitting great circle segments. The average dispersions for Categories A, B, and C are 0.9, 1.4, and 2.0 km, with respective degrees of freedom of 89, 248, and 90. The dispersions thus decrease as the marine navigation improves, much as we expected. The 2.0 km dispersion of Category C crossings is misleadingly small for cruises that lack satellite navigation because we eliminated the cruises with the largest systematic navigational offsets before we started the dispersion analysis. Using the *F*-ratio test, we found that the dispersions for the three categories differ at high confidence levels.

The distribution of normalized residual distances for the 679 anomaly crossings that we ultimately used to derive the Pacific–Rivera rota-

tions (Tables 2 and 3) is approximately Gaussian, with 68.3% of the normalized residuals located within 0.93 standard deviations of the mean (0.0). This suggests that the data uncertainties that we assigned are approximately correct and further implies that the rotation uncertainties (Table 3) derived from these data are approximately correct. We derived uncertainties for the Pacific–Mathematician anomaly crossings in an analogous manner and found uncertainties of 1.2, 2.0, and 2.8 km for Categories A, B, and C, slightly larger than for the Pacific–Rivera anomaly crossings.

### 3.3. Conjugate points and uncertainties

Given the lack of reliable fracture zone offsets along the Pacific–Rivera rise, we approximated paleo-slip directions by assuming that seafloor spreading since 10 Ma has been perpendicular to the paleo-spreading axis. Using the orientations of the seafloor spreading lineations as our guide, we constructed a flow line stretching from anomaly 5n.2 on the Pacific plate to anomaly 5n.2 on the

Table 2  
Pacific–Rivera rotations

Chron	Age <sup>a</sup> (Myr)	$\lambda$ (°N)	$\phi$ (°W)	$\omega$ (degrees)	$\chi^2_v$	$n^c$	$s$	df <sup>b</sup>
1	0.78,o	26.7	105.2	3.66	0.719	72	3	62
1r.1	1.03,c	28.0	104.4	3.98	0.859	73	3	63
2	1.86,c	30.3	102.8	4.93	0.962	82	3	72
2A.1	2.58,y	34.7	100.1	4.60	1.170	62	2	54
2A.3	3.60,o	31.3	103.2	8.63	1.195	52	1	46
3n.1	4.24,c	28.4	105.3	14.74	0.727	33	1	27
3n.2	4.63,o	27.5	105.9	18.70	0.693	32	1	26
3n.4	5.12,c	28.0	105.7	19.50	0.514	33	1	27
3A.1	6.02,y	28.7	105.6	21.21	1.138	41	1	35
3A.2	6.73,o	33.4	103.5	14.89	1.191	38	1	32
3B	7.16,c	34.0	103.2	15.23	1.806	42	1	36
4n.2	7.90,c	35.8	102.7	15.17	1.198	45	1	39
4A	8.75,y	34.7	103.9	18.45	1.311	39	1	33
5n.2	9.92,y	31.9	106.0	27.20	1.471	63	1	57

All rotations move points on the Pacific plate into their positions in a fixed Rivera reference frame. Reduced chi-square ( $\chi^2_v$ ) is the least-squares misfit  $\chi^2$  divided by the degrees of freedom  $v$  (see text). Parameters are:  $\lambda$ =rotation latitude,  $\phi$ =rotation longitude,  $\omega$ =rotation angle,  $n$ =number of anomaly crossings and conjugate points,  $s$ =the number of great circle segments,  $df$ =degrees of freedom.

<sup>a</sup> ‘o’=old edge; ‘y’=young edge; ‘c’=center. Ages are taken from Hilgen et al. (1995) with the following exceptions: ages for anomalies 3A.1 and 3A.2 are adopted from D. Wilson (pers. commun., 1999), and the age for anomaly 5n.2 is taken from Cande and Kent (1995).

<sup>b</sup> Includes two conjugate points.

Table 3  
Pacific–Rivera finite rotation covariances

Chron	<i>a</i>	<i>b</i>	<i>c</i>	<i>d</i>	<i>e</i>	<i>f</i>	<i>g</i>
1	2.53	7.18	−2.92	20.57	−8.33	3.39	10 <sup>−6</sup>
1r.1	2.40	6.70	−2.75	19.15	−7.77	3.17	10 <sup>−6</sup>
2	2.08	5.48	−2.32	15.69	−6.40	2.66	10 <sup>−6</sup>
2A.1	4.71	11.51	−5.16	33.37	−13.75	5.90	10 <sup>−6</sup>
2A.3	7.40	18.82	−8.33	53.59	−22.53	9.70	10 <sup>−6</sup>
3n.1	20.35	55.06	−24.13	154.70	−66.55	28.90	10 <sup>−6</sup>
3n.2	34.10	92.88	−40.39	258.38	−111.08	48.07	10 <sup>−6</sup>
3n.4	30.75	82.52	−35.78	227.10	−97.21	41.89	10 <sup>−6</sup>
3A.1	30.15	79.55	−34.45	215.33	−92.02	39.60	10 <sup>−6</sup>
3A.2	43.90	114.91	−49.63	306.39	−131.21	56.41	10 <sup>−6</sup>
3B	19.24	46.69	−20.69	125.06	−52.92	22.89	10 <sup>−6</sup>
4n.2	8.79	16.52	−7.76	45.36	−18.54	7.95	10 <sup>−6</sup>
4A	17.48	35.39	−15.32	93.19	−37.71	15.51	10 <sup>−6</sup>
5n.2	6.94	4.55	−2.71	16.37	−6.47	2.71	10 <sup>−6</sup>

Covariances are computed in a Pacific plate reference frame and thus describe the uncertainty in the rotated position of the Pacific plate. Covariances are Cartesian, with elements *a*, *d*, and *f* representing the variances of the (0°N, 0°E), (0°N, 90°E), and 90°N components of the best-fitting rotation (Chang, 1988; Chang et al., 1990; Royer and Chang, 1991). Units are radians<sup>2</sup>. The covariance matrix can be reconstructed as follows:

$$\begin{pmatrix} a & b & c \\ b & d & e \\ c & e & f \end{pmatrix} \cdot g.$$

Rivera plate (Fig. 3). To ensure continuity of this flow line, we extrapolated conjugate point locations for anomaly 4A on the Pacific plate and anomalies 4n.2 and 4A on the Rivera plate.

We assigned upper bounds for uncertainties in conjugate point locations as rigorously as possible. For anomaly 1, spreading has been approximately orthogonal to the rise axis (Lonsdale, 1995), with an overall spreading direction uncertainty of 1–2° (1 $\sigma$ ). For the 50 km width of anomaly 1 crossed by our flow line, a 1 $\sigma$  directional uncertainty of  $\pm 1.5^\circ$  maps into individual conjugate point uncertainties of  $\sim 1$  km. For older times, we estimated uncertainties by determining how far conjugate points can be shifted in an isochron-parallel direction without violating known paleogeographic constraints. For example, we infer an upper bound of 25 km in the relative location uncertainty of the anomaly 5n.2 conjugate pair. A shift of more than 20–25 km in the relative locations of the conjugate points forces the southernmost crossings of anomaly 5n.2 from the Rivera plate to reconstruct to a physically implausible location south of the west-

ern Clarion fracture zone on the Pacific plate. If we assume that 25 km represents a 1-D 95% (1.96 $\sigma$ ) uncertainty, then the combined 1 $\sigma$  uncertainty in the locations of the conjugate points is 12.8 km, and the uncertainty in the location of each conjugate point is 9 km.

For anomalies 3A.2 through 3n.1, we used the pseudo-fault that abruptly terminates these anomalies at their northeastern ends to estimate upper bounds on conjugate pair uncertainties (Figs. 2 and 3). In general, the intersections of the pseudo-fault with these lineations can be located to within 10 km on both sides of the spreading center (Fig. 3), thereby implying 1 $\sigma$  uncertainties of  $\sim 4$  km for the location of individual conjugate points.

Conjugate point locations for anomalies 4A, 4n.2, and 3B are more poorly known than for the other anomalies. None of these anomalies is as clearly terminated at its northern end by the pseudo-fault described above, as is the case for anomalies 3A.2–3n.1. The pseudo-fault on either side of the ridge has no clear expression in bathymetry

that we gridded from cruises in this area and, within uncertainties, could be located anywhere within 10–20 km of our best estimate (Fig. 2). We thus assigned  $1\sigma$  uncertainties for these times to allow for isochron-parallel 95% uncertainties of 15–20 km.

We modeled paleo-spreading directions for the ridge segments south of the Clarion fracture zone by assigning conjugate points that enforce ridge-normal spreading. Conveniently, these lie approximately equidistant from the Clarion fracture zone (Fig. 3) and thus obey the paleogeographic constraint that anomaly crossings south of the Clarion fracture zone not reconstruct to positions north of the Clarion. Paleo-spreading directions for a Pacific–Mathematician seafloor younger than anomaly 3n.4 are difficult to define because the abandoned ridge segments and nearby spreading lineations are partially buried beneath the volcanic flanks of Socorro and San Benedicto islands (Fig. 1). It is tempting to use the more clearly expressed spreading segments south of 18°N as a guide. However, these segments rotated CCW after anomaly 3n.4 (Mammerickx et al., 1988), and we can find no evidence for a significant CCW rotation of the northern two paleo-spreading segments. We thus infer spreading to have continued in an east–west direction (Fig. 2c) until it ceased.

#### 4. Evolution of the Pacific–Rivera paleo-rise: deformation of the Rivera plate

To determine the location and timing of internal Rivera plate deformation since 9.9 Ma (anomaly 5n.2), we compared the paleo-axial geometries that are preserved by seafloor spreading magnetic lineations on the Rivera plate to those on the presumably undeformed Pacific plate. In this section, we discuss aspects of the paleo-rise geometry that are relevant to the location and timing of deformation within the Rivera plate.

##### 4.1. Anomaly 5n.2 to 2A.3: evidence for deformation of the southern Rivera plate

Magnetic lineations from 20 to 23°N on the Pacific plate show that the Pacific–Rivera rise axis evolved from a single spreading segment at the

time of anomaly 5n.2 to at least five segments by the time of anomaly 2A.3 (Fig. 3). Anomaly 5n.2 on the Pacific plate extends north–south for nearly 250 km (Fig. 3) and is remarkably linear; the average scatter of the 63 anomaly 5n.2 crossings from their best-fitting great circle is only 1.6 km. Anomaly 5n.2 on the Rivera plate can also be traced for nearly 250 km (Figs. 2b and 3). Like its Pacific counterpart, it is linear and has only a slight CW bend along its northern end, which we attribute to localized deformation within the Rivera plate.

Anomalies 4A and 4n.2 on both sides of the rise axis consist of single, easily identified segments south of the pseudo-fault that defines the limits of the area we examined (Fig. 3), and an additional segment north of the pseudo-faults (Lonsdale, 1991). Tests of two-segment geometries for the anomaly crossings south of the pseudo-faults yield no significant improvement in the fit for any of these anomalies.

The configurations of anomalies 3B–2A.3 on the Pacific plate differ significantly from the configurations of their counterparts on the Rivera plate. On the Pacific plate, anomalies 3B, 3A.2, and 3A.1 consist of two linear segments offset by 5–10 km at ~21.0°N (Fig. 4). In contrast, anomalies 3n.4–3n.1 on the Pacific plate change azimuth by ~5° at ~21.5°N to form sideways ‘V’s that open gently to the east (Fig. 4). The ~5° bends in these lineations, though subtle, are significant — models that employ two great circle segments instead of one segment to fit the anomaly crossings for any one of these magnetic lineations show improvements in fit that are significant at a level of more than 99.99% for each of the anomalies. We attribute the slight bends in these Pacific plate lineations to slightly oblique spreading along this spreading segment, possibly in response to deformation of the Rivera plate.

On the Rivera plate, anomaly 3B is a single linear segment north of 19.75°N but is difficult to correlate farther south (Fig. 2). The magnetic lineation we tentatively interpret as anomaly 3B south of 19.75°N is rotated ~30° CW from anomaly 3B farther north and differs markedly from its Pacific plate counterpart (Fig. 4). Our tentative interpretation of anomaly 3A.2 south of 19.75°N on

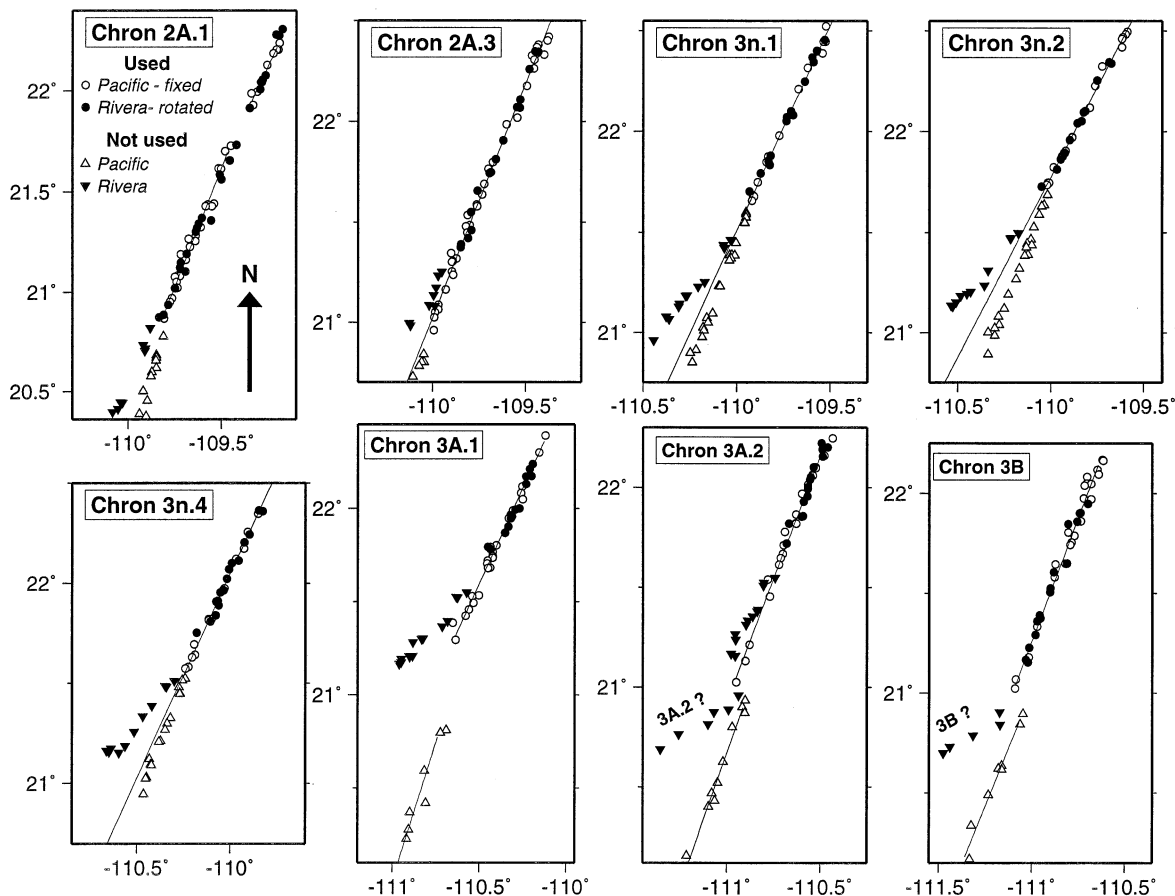


Fig. 4. Reconstructions of anomalies 2A.1 through 3B that demonstrate bending of both the Rivera- and Pacific-side lineations. Anomaly crossings shown with circles are used to solve for the best-fitting Pacific–Rivera finite rotation for a given time and are also used to solve for the best-fitting great circle segments shown in each panel. Anomaly crossings shown as triangles are not used to derive best-fitting finite rotations because they do not record Pacific–Rivera plate motion.

the Rivera plate also differs significantly from its clearly expressed counterpart on the Pacific plate. If the lithosphere on the Pacific plate is undeformed, as seems likely, this implies that the southern Rivera plate has deformed significantly sometime since the time of anomaly 3B.

Deformation of the Rivera plate may not be limited to regions south of  $\sim 19.75^\circ\text{N}$ . North of  $19.75^\circ\text{N}$  on the Rivera plate, anomalies 3A.2 through 2A.3 define sideways ‘V’s that open to the west, opposite to that observed on the Pacific plate. These ‘V’s are more sharply bent than their counterparts on the Pacific plate (Fig. 4). Given that no finite rotation can superimpose lineations

that define ‘V’s that open toward each other (Fig. 4), one or both plates had to have deformed internally between 7.2 Ma (anomaly 3B) and before 1.9 Ma (see below). The evidence that the Rivera plate deformed sometime after 7.2 Ma is compelling. Anomalies 3B–2A.3 on the Rivera plate are difficult or impossible to recognize south of  $20^\circ\text{N}$  (Fig. 2b), whereas their counterparts on the Pacific plate are easily recognized. Moreover, south of  $20^\circ\text{N}$  on the Rivera plate, magnetic lineations that might correspond to anomalies 3B and 3A.2 are rotated significantly clockwise of lineations to the north (Region A in Fig. 3). In contrast, anomalies 3B and 3A.2 on the Pacific

plate are easily recognized and show no evidence for a comparable bend north of the Clarion fracture zone.

Crossings of anomaly 2A.1 define four major paleo-spreading segments on both plates (Fig. 2) and exhibit none of the bends that affect the older anomalies. Deformation of the southern half of the Rivera plate thus ceased by 2.58 Ma. More limited deformation of the southernmost Rivera plate may, however, have occurred at this time — crossings of anomaly 2A.1 that flank the southernmost spreading segment show less opening than expected from crossings of anomaly 2A.1 farther north. Fitting crossings of anomaly 2A.1 from the southernmost segment and northern segments separately and simultaneously shows that this spreading deficit is significant at a very high confidence level (>99%). Therefore, if we have correctly interpreted these poorly expressed anomalies (Fig. 2b), spreading across the southern segment did not yet record rigid Pacific–Rivera motion at the time of anomaly 2A.1.

#### 4.2. Anomaly 2 to present: evidence for detachment of the northern Rivera plate

The paleo-axial geometry for times after anomaly 2A.1 is well defined by both the numerous crossings of these anomalies and Lonsdale's (1995) synthesis of near-ridge multi-beam, bathymetric, and marine magnetic data. Lonsdale concludes that the rise axis since anomaly 1r.1 has consisted of four major spreading segments, the northernmost of which is sub-divided into three minor segments with several km offsets (Fig. 5). We adopt this segmentation for our analysis.

Lonsdale (1995) proposes that the northwestern part of the boundary between the Rivera and North American plates, traditionally assumed to coincide with the Tamayo fracture zone (Fig. 1), jumped south sometime after 1.5 Ma to a location coincident with two recently discovered zones of normal faults that extend ESE from near the Pacific–Rivera rise at 22°N and 22.5°N. In support of this hypothesis, DeMets and Wilson (1997) use 123 crossings of anomaly 1 along the Pacific–Rivera rise to demonstrate that the lithosphere

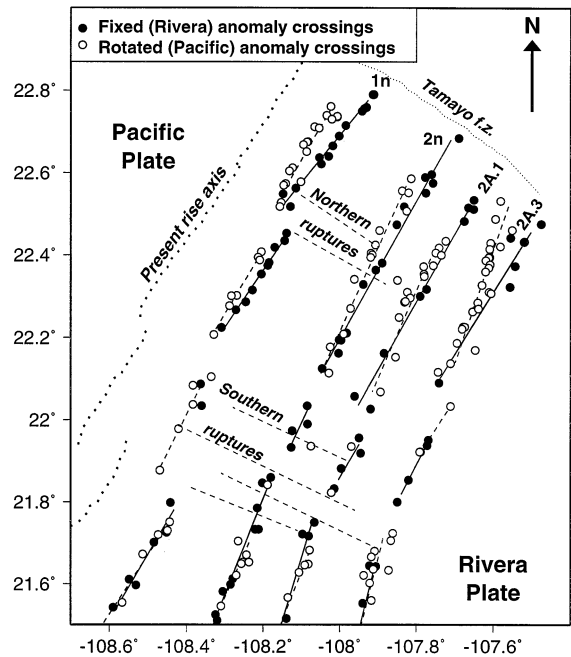


Fig. 5. Test for significant motion across rupture zones described by Lonsdale (1995). Rotations that are derived only from anomaly crossings located south of the southernmost rupture zone are used to reconstruct crossings of anomalies 1, 2, 2A.1, and 2A.3 on the Pacific plate (open circles). The rotated crossings would coincide with their fixed counterparts (solid circles) if no deformation had occurred east of the rise axis. Instead, the Pacific plate magnetic lineations are under-rotated with respect to their counterparts, with the degree of under-rotation generally increasing as a function of distance north of the southern rupture zone.

north of the southern rupture zone has sutured to the North American plate.

Fig. 5 shows crossings of anomalies 1, 2, 2A.1, and 2A.3 that have been rotated from the Pacific plate using finite rotations derived solely from Pacific–Rivera anomaly crossings located south of the southern rupture zone. If the Rivera plate has been rigid since anomaly 2A.3, then anomaly crossings rotated from the undeformed Pacific plate should rotate onto their counterparts on the Rivera plate. Instead, the rotated anomaly crossings north of the southern rupture zone are under-rotated by up to 6 km relative to their fixed counterparts (Fig. 5). The seafloor located between the southern rupture zone and eastern Tamayo fracture zone thus moved significantly

with respect to the rigid interior of the Rivera plate sometime after anomaly 2A.3, in accord with Lonsdale’s hypothesis and results presented by DeMets and Wilson (1997). We thus do not use anomaly crossings from the northernmost Pacific–Rivera rise to solve for Pacific–Rivera finite rotations.

4.3. *Timing of internal Rivera plate deformation*

The results described above provide useful constraints on the timing and extent of the deformation that affected much of the southern half of the Rivera plate. Deformation could not have begun earlier than 7.2 Ma (anomaly 3B) because anomaly 3B is the first anomaly east of the rise axis that is clearly deformed with respect to its counterpart on the Pacific plate (Fig. 4). Deformation ceased by 1.86 Ma (anomaly 2) because the numerous crossings of anomaly 2, which extend south to the edge of the present Rivera transform valley, are well fit by a single rotation (described below). For reasons enumerated below, we propose that most of the deformation started after 3.3 Ma and ended

by 2.2 Ma, when the Rivera transform fault was clearly established as the southern boundary of the Rivera plate.

5. Plate motions since 10 Ma

5.1. *Pacific–Rivera finite rotations and stage velocities*

Inversion of the conjugate points and magnetic anomaly crossings from undeformed areas of the Rivera plate (described above) and their counterparts from the Pacific plate for each of 14 times gives best-fitting finite rotations and their covariances (Tables 2 and 3). Pacific–Rivera pole locations are generally well constrained (Fig. 6) and lie 7–16 angular degrees NNE of the geographic center of the Pacific–Rivera rise. Our pole locations are consistent within uncertainties with those from prior studies (DeMets and Stein, 1990; Bandy, 1992; Bandy and Pardo, 1994; Lonsdale, 1995; DeMets and Wilson, 1997), although poles pub-

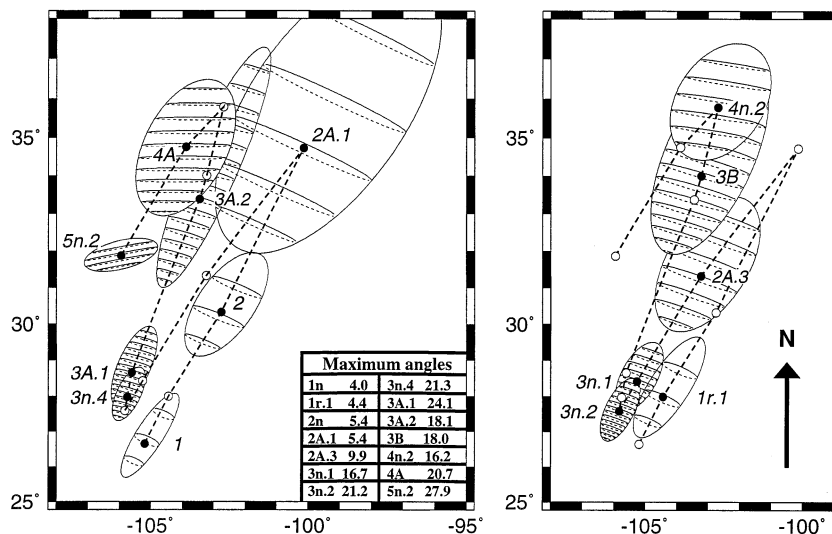


Fig. 6. Pacific–Rivera finite rotations and 3-D 95% confidence regions for all 14 times given in Table 2. Contours of the rotation angles along the upper and lower surfaces of the 95% confidence region are shown with solid and dotted lines, respectively. Adjacent contours are spaced by 0.4°. The inset in the left panel specifies the maximum rotation angle contour for each confidence region; the maximum angles always correspond to the southernmost contour associated with a given confidence region. The bold dashed line connects the time series of finite rotation axes, which are shown as solid and open circles depending on whether the corresponding confidence region is shown.

lished by previous authors are limited to times younger than 3.5 Ma.

Changes in the pole locations through time are significant at high confidence levels (>99%), thereby indicating that they record significant changes in Pacific–Rivera motion. Typical 95% uncertainties in the locations of anomaly crossings reconstructed with these rotations are only 0.4–1.0 km in the direction orthogonal to the isochrons. The isochron-parallel uncertainties in the reconstructed anomaly locations are larger, with minimum and maximum 95% reconstruction uncertainties of 2.2 km for anomaly 1 and 26 km for anomaly 5n.2. These reflect the larger uncertainties that we assigned to conjugate point locations.

Fig. 7 summarizes the geometric evolution of the rise axis since 9.9 Ma and shows the reconstructed fits of all the points used to derive the best-fitting rotations. The scatter of the anomaly crossings is relatively constant for different times (also see values of reduced chi-square in Tables 2

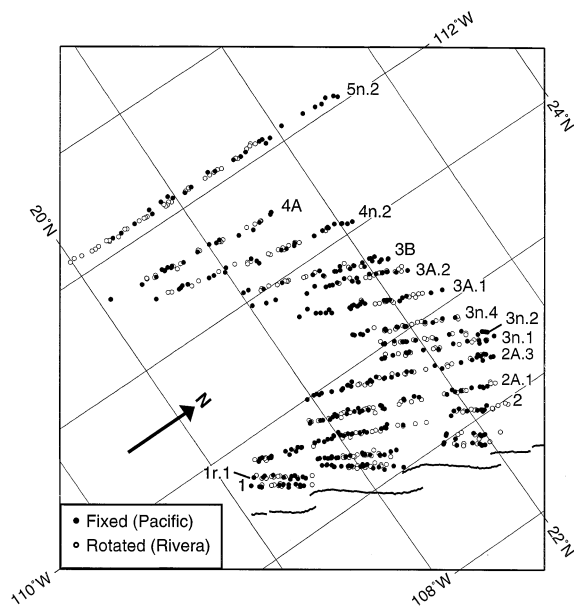


Fig. 7. Summary reconstruction of anomaly crossings used to derive the Pacific–Rivera finite rotations (Table 2). The map projection is transverse Mercator with an equatorial azimuth that parallels the present rise axis (solid line). Departures of the reconstructed magnetic lineations from horizontal thus reflect rotation of the rise axis through time.

and 3), with the northernmost crossings of anomaly 3B showing the most scatter. The summary reconstruction clearly shows that the rise axis rotated clockwise relative to the Pacific plate since 9.9 Ma. Further examination shows that the clockwise rotation was not gradual, but occurred in two principal stages, between anomaly 5n.2 and 3B, and between anomaly 2 and the present. This pattern is also clearly exhibited by the stage spreading directions (Fig. 8), which indicate that the

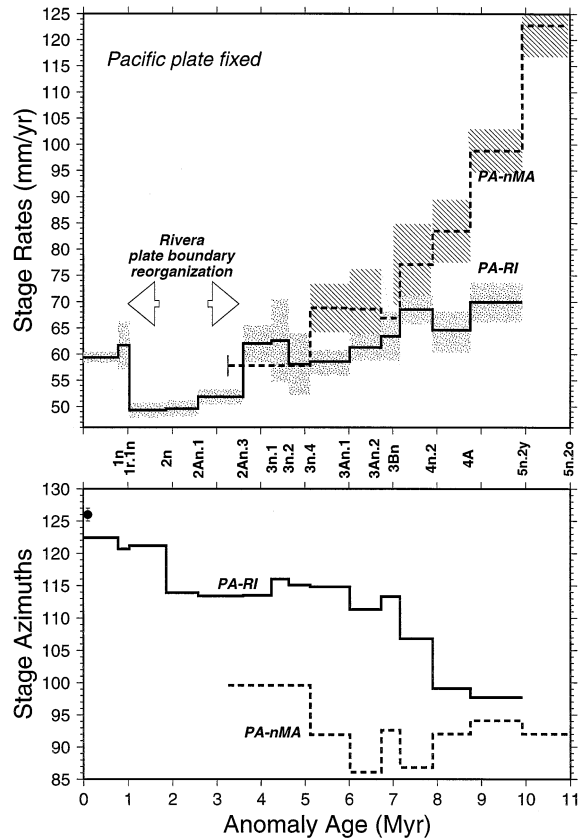


Fig. 8. Pacific–Rivera (PA–RI) and Pacific–northern Mathematician (PA–MA) stage spreading rates and azimuths out to anomaly 5n.2. Stippled and diagonal patterns show 95% uncertainties derived from the Pacific–Rivera and Pacific–northern Mathematician stage rotation covariances. Pacific–Rivera and Pacific–northern Mathematician velocities and uncertainties are computed in a fixed Pacific reference frame along their respective conjugate point flow lines on the Pacific plate (Fig. 3). Stage spreading rate uncertainties are minimum estimates that exclude uncertainties in magnetic reversal ages (see text).

paleo-axis rotated  $15^\circ$  CW between 9.92 and 7.16 Ma (anomalies 5n.2 and 3B), maintained an almost constant orientation from 7.16 to 1.86 Ma (anomalies 3B and 2), and rotated a further  $10^\circ$  CW between 1.86 Ma and the present.

To predict stage spreading rates and directions, we derived stage rotations from the best-fitting finite rotations. Uncertainties in the stage velocities are rigorously propagated from the stage rotation covariances but do not incorporate uncertainties in the ages of magnetic reversals, which are poorly known and are likely to be highly correlated for time-adjacent anomalies. Because of this, our stage rate uncertainties are minimum estimates. We also note that our discrete sampling of the continuous displacement history, consisting of 14 irregularly spaced times since 9.9 Ma, limits our ability to determine precisely when changes occurred in stage rates and directions. More precise times for the kinematic changes that we describe below will require analysis of the abyssal hill fabric and faults mapped by swath bathymetry. Because abyssal hill ages can be estimated via interpolation from nearby magnetic reversals, changes in their orientations can be used to more precisely date changes in Pacific–Rivera seafloor spreading and Rivera plate deformation. Swath bathymetry has already been used to describe the evolution of the rise axis since  $\sim 2$  Ma (Lonsdale, 1995) and will undoubtedly play a major role in furthering our understanding of Rivera plate kinematics for older times.

Stage spreading rates (Fig. 8) calculated along the flow line shown in Fig. 3 exhibit several significant changes over the past 10 Ma. From 9.9 to 3.6 Ma (anomaly 5n.2 to anomaly 2A.3), full spreading rates declined gradually from  $70 \pm 5$  to  $63 \pm 3$  mm/yr (this and all subsequent uncertainties are 95% unless otherwise noted). During this time, rates were well behaved, never varying more than  $\sim 5$  mm/yr from one interval to the next. This supports the joint hypotheses that rates varied little during this period and that errors in estimates of reversal ages during this period are not a serious source of error. Moreover, it suggests that the formal stage rate uncertainties of several mm/yr (Fig. 8) are approximately correct.

Following this long period of slowly declining spreading rates, spreading rates slowed rapidly to

$49\text{--}53 \pm 1$  mm/yr and remained slow until 1.0 Ma (anomaly 1r.1). After  $\sim 1$  Ma, spreading accelerated to  $60 \pm 2$  mm/yr along the flow line, approximately the same as for times prior to 3.6 Ma. Spreading rates since 0.78 Ma range from  $51 \pm 2$  mm/yr at the northern limit of Pacific–Rivera seafloor spreading to  $70 \pm 2$  mm/yr near the Rivera transform fault. Given that uncertainties in magnetic reversal ages for the past few Myr are typically 0.01–0.02 Myr (Wilson, 1993b; Hilgen et al., 1995) and that stage rates for times younger than 3.6 Ma are averaged over intervals from 0.25–1.02 Myr, reversal age uncertainties would increase the formally estimated stage rate uncertainties only minimally if we accounted for them. Consequently, we view the evidence for a period of slow seafloor spreading from 3.6 to 1.0 Ma and a spreading acceleration after 1.0 Ma as extremely robust.

### 5.2. Pacific–northern Mathematician stage velocities

To describe the spreading history of the Mathematician ridge just south of the Clarion fracture zone, we derived finite and stage rotations and covariances from 120 anomaly crossings and eight conjugate pairs that flank the northern Mathematician ridge (Table 4). For reasons described above, we used only magnetic anomaly crossings located north of about  $18^\circ\text{N}$  to solve for Pacific–northern Mathematician motion. Consequently, the rotations in Table 4 are only suitable for describing ridge-normal seafloor spreading rates across the two now-extinct Pacific–Mathematician seafloor spreading segments immediately south of the Clarion fracture zone.

The most notable feature of seafloor spreading along the northern Mathematician ridge is the dramatic slowdown in stage spreading rates (Fig. 8) from 11 Ma (the old edge of anomaly 5n.2) to 7 Ma (anomaly 3B). During this period, full spreading rates decreased by nearly 50%, from  $123 \pm 4$  to  $64 \pm 13$  mm/yr. Spreading rates after  $\sim 7$  Ma appear to have remained relatively constant. The magnetic anomalies adjacent to these now-extinct spreading segments (Fig. 2c) suggest that spreading ceased about  $3.28 \pm 0.05$  Ma, the midpoint of the reversed polarity epoch that sepa-

Table 4  
Pacific–northern Mathematician rotations and covariances

Chron	$\lambda$ ( $^{\circ}$ N)	$\phi$ ( $^{\circ}$ W)	$\omega$ (degrees)	$\chi^2_v$	$n^a$	$s$	df <sup>a</sup>	$a$	$b$	$c$	$d$	$e$	$f$	$g$
3n.4	27.7	109.7	−6.29	0.96	17	1	11	15.8	41.5	−15.2	111.9	−40.9	15.0	10 <sup>−4</sup>
3A.1	11.1	111.9	10.74	1.10	17	1	11	24.5	66.7	−24.3	181.2	−66.2	24.1	10 <sup>−4</sup>
3A.2	12.2	111.7	16.08	0.83	19	1	13	41.8	115.0	−41.5	317.0	−114.5	41.4	10 <sup>−6</sup>
3B	6.4	112.4	9.98	1.00	15	1	9	14.2	39.3	−14.3	109.4	−39.8	14.5	10 <sup>−5</sup>
4n.2	8.2	112.1	14.29	1.15	16	1	10	96.6	268.1	−97.6	758.3	−274.2	99.5	10 <sup>−6</sup>
4A	5.3	112.6	14.02	1.44	16	1	11	68.5	192.1	−69.2	553.8	−197.5	70.7	10 <sup>−6</sup>
5n.2(y)	−5.0	114.0	10.69	0.64	18	1	12	53.2	152.9	−54.5	454.6	−159.9	56.6	10 <sup>−6</sup>
5n.2(o)	−16.7	115.6	9.39	0.47	18	1	12	39.9	113.5	−39.2	349.1	−117.9	40.1	10 <sup>−6</sup>

All rotations move points on the Mathematician into their positions in a fixed Pacific plate reference frame. See footnotes to Table 2 for additional information. Covariances describe the uncertainty in the position of a point on the Mathematician plate rotated onto the Pacific plate. See footnotes to Table 3 for further information.

<sup>a</sup> Includes two conjugate points.

rates the end of anomaly 2A.3 (3.33 Ma) and the beginning of anomaly 2A.2 (3.22 Ma).

The Pacific–Rivera and Pacific–Mathematician rates (and directions) described above clearly did not change in tandem prior to  $\sim 5$  Ma (Fig. 8), as one might expect if the Rivera and Mathematician plates were part of a single rigid plate. We conclude that the northernmost Mathematician plate was not rigidly coupled to the Rivera plate at any time after 10 Ma. The often-asserted concept that the Rivera plate initiated its existence as an independent microplate at  $\sim 5$  Ma when it broke away from the Cocos plate (Lonsdale, 1991, 1995; Stock and Lee, 1994) thus requires modification — the Rivera plate has existed as an independent microplate since at least 10 Ma.

### 5.3. Plate reconstructions

We next show paleogeographic reconstructions of the Rivera, northern Mathematician, and North American plates relative to the Pacific plate since 10 Ma using the finite rotations from Tables 2–5 and Pacific–North America rotations described below (Fig. 9). We reconstructed magnetic lineations that flank the abandoned spreading segment north of the Clarion fracture zone using rotations derived from the anomaly crossings flanking that segment. All features on the Pacific plate are in place.

Our reconstructions differ from, and complement, those of Lonsdale (1989, 1991, 1995) in two

respects: they are easily reproduced using rotations from Tables 2, 4 and 5, and they minimize extrapolations of features beyond the extent of the available data and thus emphasize where gaps in our knowledge remain. We did not reconstruct the location of the Baja peninsula prior to anomaly 3A.2; the peninsula was moving slowly northwest away from the North American plate (e.g. Stock and Lee, 1994) and its location can only be approximated. We also did not reconstruct details of seafloor spreading along the Maria Magdalena rise, which created a sequence of NNE-trending magnetic lineations (Fig. 2b) that record the earliest seafloor spreading between the Baja peninsula and western Mexico (Lonsdale, 1989). Finally, our reconstructions do not display the still poorly understood history of internal deformation of the Rivera plate, which awaits a synthesis of the many multi-beam data that image the Rivera plate.

Hereafter, we assume that the Jalisco block has moved with the North American plate and thus do not attempt to restore motion across faults that bound the Jalisco block or faults farther inland. Most evidence argues against significant motion of the Jalisco block relative to North America since at least  $\sim 5.5$  Ma. The general absence of seismicity in northern and central Mexico and evidence that GPS stations in western Mexico are moving as part of the stable interior of the North American plate (C. DeMets and B. Marquez-Azua, work in progress, 1999) indicates that the present deformation is slow or zero. At  $\sim 5.5$  Ma, Pacific–

Table 5  
Rivera–North America rotations and covariances

Chron	$\lambda$ ( $^{\circ}$ N)	$\phi$ ( $^{\circ}$ E)	$\omega$ (degrees)	$a$	$b$	$c$	$d$	$e$	$f$	$g$
<i>Maximum and minimum change<sup>a</sup></i>										
1	21.7	251.3	−3.16	24.5	70.7	−28.3	207.4	−82.8	33.3	10 <sup>−7</sup>
1r.1	22.1	251.2	−3.31	23.1	65.6	−26.4	193.5	−77.1	31.0	10 <sup>−7</sup>
2	21.6	250.7	−3.72	19.9	53.0	−21.5	159.9	−63.2	26.0	10 <sup>−7</sup>
2A.1	21.8	249.0	−2.87	44.3	109.9	−46.9	341.5	−135.7	56.8	10 <sup>−7</sup>
<i>Maximum change<sup>a</sup></i>										
2A.3	21.2	249.6	−6.31	74.6	185.0	−78.5	561.2	−226.5	97.1	10 <sup>−7</sup>
3n.1	21.0	250.5	−12.08	185.5	523.2	−217.6	1613.1	−660.1	277.3	10 <sup>−7</sup>
3n.2	21.0	250.8	−15.83	297.2	869.3	−356.8	2697.2	−1096.9	454.3	10 <sup>−7</sup>
3n.4	21.0	250.7	−16.33	265.9	767.6	−311.8	2388.4	−960.7	396.4	10 <sup>−7</sup>
3A.1	20.9	250.7	−17.49	256.1	731.5	−293.5	2293.4	−910.8	374.6	10 <sup>−7</sup>
3A.2	21.4	249.1	−10.61	350.9	1032.3	−411.9	3279.5	−1295.7	528.2	10 <sup>−7</sup>
3B	21.5	249.0	−10.67	177.7	436.3	−176.9	1370.7	−534.2	227.1	10 <sup>−7</sup>
4n.2	22.1	248.2	−10.08	111.6	180.8	−74.1	536.6	−203.3	98.9	10 <sup>−7</sup>
4A	22.0	248.4	−12.89	174.1	341.3	−126.5	1070.6	−394.3	171.9	10 <sup>−7</sup>
5n.2(y)	21.6	249.3	−21.06	123.1	110.1	−27.5	263.6	−92.9	71.9	10 <sup>−7</sup>
<i>Minimum change<sup>a</sup></i>										
2A.3	21.4	249.5	−6.29	83.5	192.6	−82.4	570.3	−230.8	103.3	10 <sup>−7</sup>
3n.1	21.4	250.4	−12.04	185.5	523.2	−217.6	1613.1	−660.1	277.3	10 <sup>−7</sup>
3n.2	21.3	250.7	−15.79	297.2	869.3	−356.8	2697.2	−1096.9	454.3	10 <sup>−7</sup>
3n.4	21.4	250.7	−16.28	265.9	767.6	−311.8	2388.4	−960.7	396.0	10 <sup>−7</sup>
3A.1	21.6	250.6	−17.42	256.1	731.5	−293.5	2293.4	−910.8	374.6	10 <sup>−7</sup>
3A.2	22.8	249.0	−10.52	350.9	1032.3	−411.9	3279.5	−1295.7	528.2	10 <sup>−7</sup>
3B	23.0	248.9	−10.58	177.7	436.3	−177.0	1370.7	−534.2	227.1	10 <sup>−7</sup>
4n.2	24.0	248.1	−9.98	68.3	139.9	−55.4	483.7	−182.2	69.0	10 <sup>−7</sup>
4A	22.7	248.4	−13.07	205.1	445.5	−164.4	1420.4	−522.1	218.6	10 <sup>−7</sup>
5n.2(y)	21.5	249.4	−21.06	123.5	110.0	−27.3	263.6	−92.9	71.9	10 <sup>−7</sup>

All rotations move points on the Rivera into their positions in a fixed North American plate reference frame. See footnotes to Table 2 for additional information. Covariances describe the uncertainty in the position of a point on the Rivera plate rotated onto the North American plate. See footnotes to Table 3 for further information.

<sup>a</sup> Rotations derived using maximum and minimum change rotations for Pacific–North America motion. See text for further details.

North America plate motion transferred to faults in the Gulf of California that were favorably oriented to carry all or nearly all motion between the two plates (Stock and Hodges, 1989), thereby precluding the need for significant extension within the Basin and Range east of the Gulf of California after this time. Displacements across the Colima graben and Tepic–Zacoalco fault zone, which separate the Jalisco block from the North American plate, appear to have been no more than a few per cent of overall Rivera–North America displacement since 10 Ma (Allan, 1986; Ferrari et al., 1994; Righter et al., 1995) and thus play a minor role in decoupling the Jalisco block from North America. The greatest source of uncertainty is whether dis-

tributed slip across either the Trans-Mexican volcanic belt (Pasquare et al., 1988) or the Basin and Range province of central Mexico (Stock and Hodges, 1989; Henry and Aranda-Gomez, 2000, this volume) prior to  $\sim 5.5$  Ma decoupled the Jalisco block from North America. A synthesis of original and published geologic and structural observations from the southern Basin and Range province adjacent to, and east of, the Jalisco block suggests, however, that only minor extension has occurred since  $\sim 11$  Ma (Nieto-Samaniego et al., 1999). The evidence at present thus suggests that our assumption of negligible motion between the Jalisco block and North America since 9.9 Ma (anomaly 5n.2) is adequate.

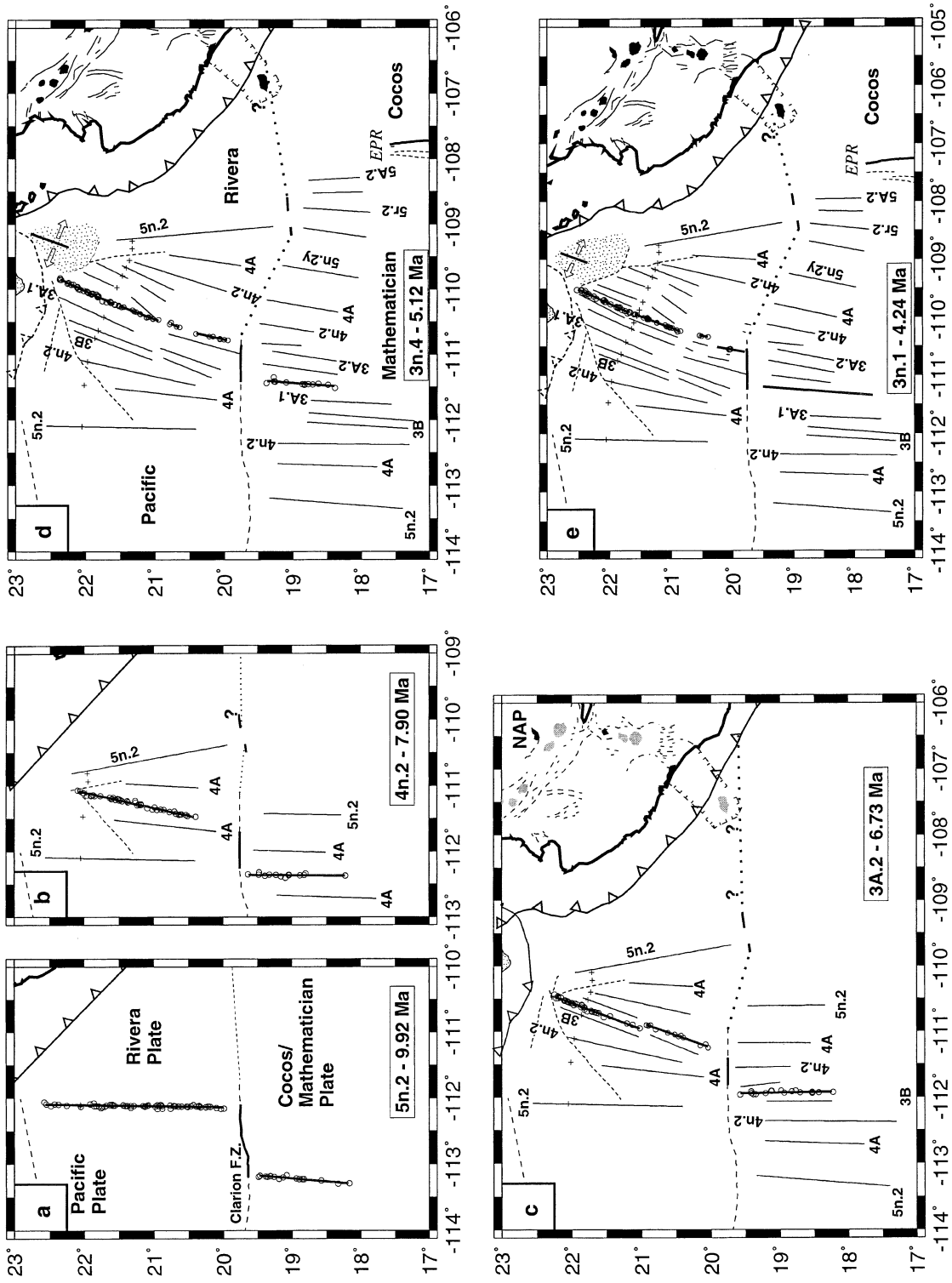


Fig. 9.

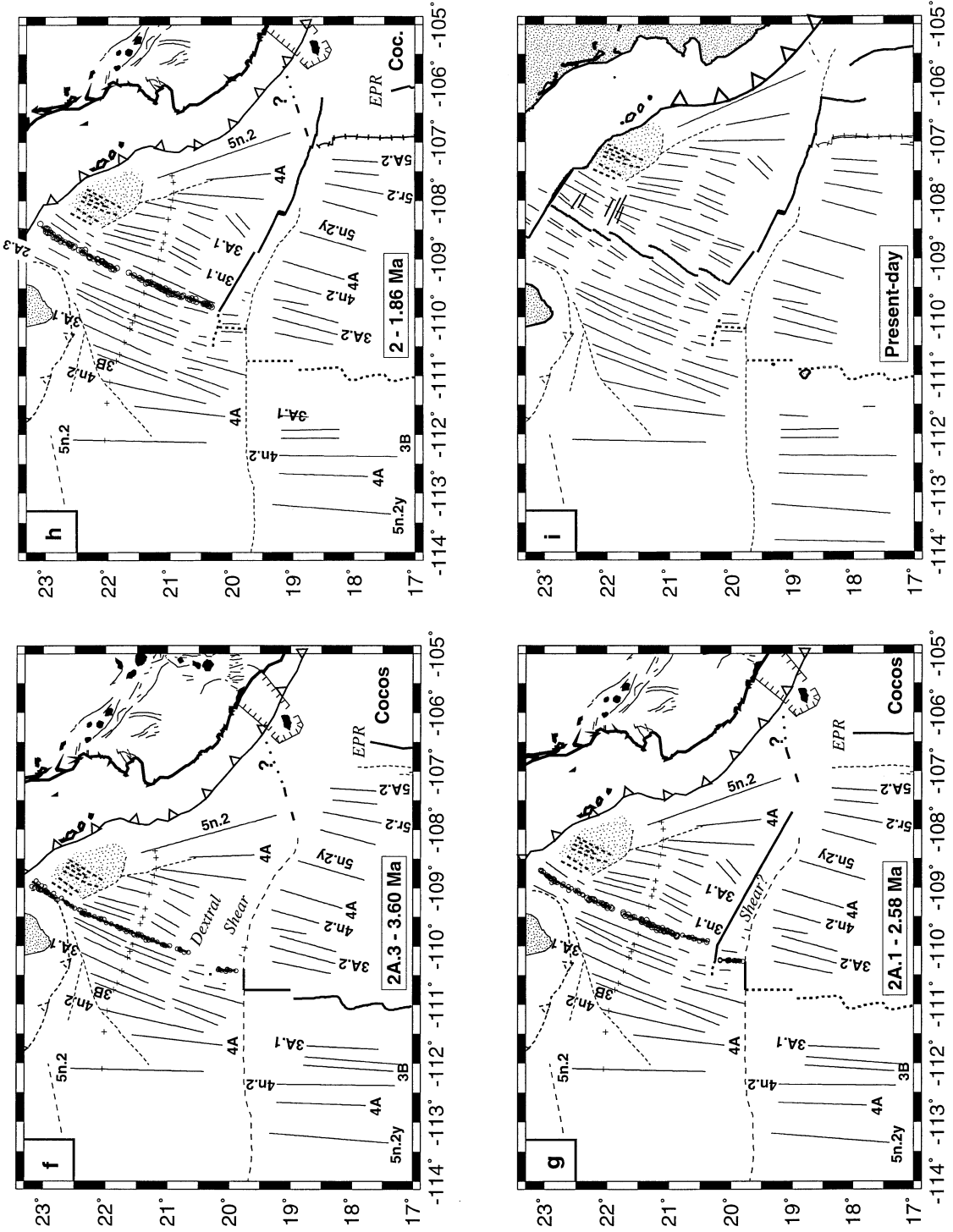


Fig. 9. (continued)

### 9.9–6.7 Ma: anomalies 5n.2–3A.2

At 9.92 Ma (Fig. 9a), the Pacific–Riviera rise consisted of a single spreading segment bounded to the north by the fault that marked the southern boundary of the Magdalena microplate (Lonsdale, 1991; Stock and Lee, 1994) and to the south by the Clarion fracture zone. Reconstructing the southernmost crossings of anomaly 5n.2 from the Rivera plate onto the Pacific plate places them ~20 km north of the western Clarion fracture zone. We thus infer that any remnant of the Clarion fracture zone near the Middle America trench must be located ~20 km south of the southernmost crossings of anomaly 5n.2 on the Rivera plate.

Clockwise rotation of the Pacific–Riviera rise commenced after 9.92 Ma and continued until 7.2 Ma (Fig. 7–9c). Seafloor spreading rates remained relatively constant during this period. In contrast, the orientation of the northern Mathematician rise remained constant during this period, but seafloor spreading rates slowed by more than 50%. The Rivera and Mathematician

plates thus moved as separate plates during this period (and thereafter).

### 5.1–4.2 Ma: anomalies 3n.4 and 3n.1

After 5.1 Ma, the spreading segment just north of the Clarion fracture zone (Fig. 9d–e) began rotating CCW into an orientation similar to that of the northern Mathematician ridge (Lonsdale, 1995), and seafloor spreading along this segment became distinctly slower than predicted by both the Pacific–Riviera and Pacific–northern Mathematician stage rotations for the interval 5.1–3.6 Ma. This suggests that the seafloor immediately east of this segment acted as a microplate, possibly until spreading ceased along its western edge at ~2.2 Ma. The eastern edge of this microplate, if it existed, was presumably a zone of distributed deformation associated with the nascent Rivera transform fault. The combination of slower spreading and CCW rotation of this spreading segment increased its westward offset from the southern Pacific–Riviera rise and required the formation and lengthening of a short-offset transform fault that

Fig. 9. Post-10 Ma Rivera, Mathematician, and North America plate reconstructions in a fixed Pacific reference frame. Seafloor spreading lineations are represented by great circle segments that best-fit the anomaly crossings shown in Fig. 3. Paleo-spreading centers and paleo-plate boundaries are shown with bold lines. Open circles show anomaly crossings with ages equal to that for the reconstruction. Crosses define the Pacific–Riviera flow line. In all reconstructions after anomaly 5n.2, the dashed line south of anomaly 5n.2 on the Rivera plate is the Clarion fracture zone rotated from the Pacific plate and is used as an approximate marker of the eastern Clarion fracture zone. (a) Anomaly 5n.2. Subduction zone locations in this and the following panel are schematic. Rivera and Cocos plates are shown as distinct due to significantly different stage spreading rates along seafloor spreading segments north and south of the Clarion fracture zone (Fig. 8). (b) Anomaly 4n.2. The short dashed line shows the trail of a propagating rift that originated at approximately 8.8 Ma (anomaly 4A). (c) Anomaly 3A.2. The North American plate (NAP) and present-day trench axis are rotated into a fixed Pacific plate reference frame in this and all subsequent frames using Pacific–North America rotations described in text. (d) Anomaly 3n.4. Seafloor spreading along the Maria Magdalena rise near the mouth of the Gulf of California (stippled region) (Lonsdale, 1995) produced lineated magnetic anomalies now located near 21.5°N, 253°E (Fig. 2b). In this and subsequent panels, northward propagation of the East Pacific rise (EPR) and the corresponding position of the Moctezuma trough (dashed lines just west of the EPR) are constrained using results from Mammerickx et al. (1988), all rotated into the Pacific reference frame. (e) Anomaly 3n.1. The now-abandoned spreading axis just north of the western Clarion fracture zone aligns well with the two northernmost Mathematician ridge spreading segments but has stage spreading rates that are intermediate between rates predicted by Pacific–Riviera and Pacific–northern Mathematician stage rotations. (f) Anomaly 2A.3. The Mathematician spreading center (bold dotted line) ceased spreading shortly after this time, thereby imposing rapid dextral shear between the southernmost Pacific–Riviera rise and the northernmost East Pacific rise. The Moctezuma trough (line with tic marks) divides seafloor created along the Pacific–Cocos and northern Mathematician spreading centers. (g) Anomaly 2A.1. An opening deficit along the southernmost Pacific–Riviera rise segment indicates that the southernmost Rivera plate was still deforming at this time, and spreading across the abandoned rise axis north of the Clarion fracture zone ceased at 2.2 Ma. Together, these indicate that dextral shear between the Pacific and Rivera plates was not confined to the Rivera transform fault until after 2.2 Ma. (h) Anomaly 2. Crossings of anomaly 2 clearly extend to the northern edge of the Rivera transform valley and are well fit by a single rotation, thereby indicating that all Rivera plate deformation north of the Rivera transform valley had ceased by this time. (i) Present-day. Clockwise rotation of the rise axis after anomaly 2 resulted in further segmentation of the rise axis, and ESE-trending ruptures within seafloor north of 22°N appear to have detached seafloor north of the rupture zones from the rigid Rivera plate (Lonsdale, 1995).

connected the two spreading axes, as previously recognized by Lonsdale (1995).

*3.6–2.6 Ma: anomalies 2A.3–2A.1: dextral shear and the birth of the Rivera transform fault*

After 4.2 Ma, a series of profound and presumably related changes in the regional kinematics occurred (Fig. 9f and g). Seafloor spreading ceased along the northern Mathematician ridge at  $\sim 3.3$  Ma (Klitgord and Mammerickx, 1982), thereby suturing the Mathematician plate to the Pacific plate. This reversed the sense of shear along the southern paleoboundary of the Rivera plate from slow left-lateral motion prior to 3.3 Ma to  $\sim 70$  mm/yr of dextral shear after 3.3 Ma. It seems likely that the significant decrease in Pacific–Rivera stage spreading rates during this period (Fig. 8) was a kinematic response to the onset of distributed right-lateral shear along the southern edge of the Rivera plate and the difficulty in translating Rivera lithosphere eastward away from the spreading axis in the absence of a well-defined transform fault between the two plates. An alternative explanation, that the spreading deceleration was part of a regional slowdown in seafloor spreading, conflicts with strong evidence for constant Pacific–Cocos spreading rates since 3.5 Ma (Wilson, 1993b).

From 3.3 to 2.2 Ma, dextral shear along the southern edge of the Rivera plate was presumably partitioned between the Clarion transform fault, the nascent Rivera transform fault, and distributed deformation in the Rivera plate that extended as far north as the prominent bends in anomalies 3A.1–2A.3 (Fig. 4). Seafloor spreading continued until  $\sim 2.2$  Ma across the rise segment located just north of the Clarion fracture zone at an average rate of  $34 \pm 1$  mm/yr (Fig. 9g). This is significantly slower than the  $64 \pm 4$  mm/yr Pacific–Rivera stage rate predicted for this location at this time. The spreading rate differential between the two requires there to have been significant additional deformation somewhere east of this short segment from 3.3 to 2.2 Ma, presumably within the southern Rivera plate or along its evolving southern boundary. The cessation of spreading at  $\sim 2.2$  Ma along this short segment marks the time by which most or all Pacific–Rivera motion had shifted to the

Rivera transform valley. In support of this interpretation, we note that the previously described spreading ‘deficit’ for anomaly 2A.1 along the southernmost Rivera rise indicates that the southernmost Rivera plate was still partially decoupled from its rigid interior after 2.6 Ma.

*1.86 Ma: anomaly 2*

The numerous crossings of anomaly 2 extend nearly to the edge of the present Rivera transform valley (Fig. 3) and are well fit by a single rotation. This requires that distributed deformation of the southern Rivera plate ceased no later than 1.86 Ma. This in turn implies that nearly all Pacific–Rivera dextral shear was being accommodated within, or south of, the Rivera transform fault by this time. After 1.86 Ma, any faults that had previously accommodated some of this dextral shear were frozen into the southern Rivera plate and may have been dissected by the Rivera transform fault. Identifying any such features and realigning them with their continuations south of the present transform valley would provide useful additional constraints on the time that the Rivera transform fault adopted its present form.

*5.4. Linking the Rivera plate to North America*

To derive estimates of Rivera–North America motion (Table 5), we combined our estimates of Rivera–Pacific motion (Tables 2 and 3) with newly available rotations that describe motion of the Pacific plate relative to North America (J. Stock, pers. commun., 1999; DeMets and Dixon, 1999). The uncertainties in Rivera–North America motion are small for times from 3.6 Ma to the present because Pacific–Rivera and Pacific–North America motions during this period are estimated with numerous data that have well-understood uncertainties [see Tables 2 and 3, and DeMets and Dixon (1999)]. Results for times since 3.6 Ma are thus likely to be robust. Estimates of Rivera–North America motion for times prior to 3.6 Ma would benefit significantly from a reduction of the still-large uncertainties in Pacific–North America rotations and improved temporal resolution. Such a task is beyond the scope of this paper because it

requires analysis of magnetic anomaly and fracture zone crossings from a global plate circuit.

### 5.5. Pacific–North America motion

To describe the motion of the Pacific plate relative to North America, we use rotations for three times since 11 Ma: the old edge of anomaly 5n.2 (10.95 Ma), the center of anomaly 2A.2 (3.16 Ma), and 0.0 Ma (a geodetic average). The former rotation was derived by reconstructing anomaly and fracture zone crossings from the Pacific–Antarctic–Africa–North America plate circuit (J. Stock, pers. commun., 1999). The latter two rotations were derived from seafloor spreading rates, transform fault and earthquake slip directions, and geodetically measured station velocities from a global plate circuit (DeMets and Dixon, 1999). These are the only Pacific–North America rotations for times since 11 Ma for which uncertainties are available.

At 19°N, 105.5°W along the northern Middle America trench, the 0.0 and 3.16 Ma rotations predict respective velocities of  $55.7 \pm 1.6$  mm/yr toward N60°W  $\pm 1.8^\circ$  and  $54.1 \pm 1$  mm/yr toward N60°W  $\pm 1^\circ$ . These are the same within the uncertainties, thereby suggesting that motion since 3.16 Ma has remained constant (DeMets and Dixon, 1999). The 10.95 Ma finite rotation predicts an average velocity for the North American plate of  $58.3 \pm 1$  mm/yr toward N63°W  $\pm 1.5^\circ$ . The velocities averaged over 0.0 and 3.16 Ma are thus 3–4 mm/yr slower than the velocity averaged over 10.95 Ma, but are in the same direction within uncertainties.

To determine whether the 3–4 mm/yr difference in the velocities predicted by the finite rotation for anomaly 5n.2 and the 0.0 Ma and 3.16 Ma-average rotations is indicative of a decrease in Pacific–North America rates since 10.9 Ma or instead reflects the underlying noise, we also examined the predictions of two additional intermediate-age rotations, one for anomaly 4n.2 (7.90 Ma) and the other for anomaly 3n.4 (5.12 Ma) (J. Stock, pers. commun., 1999). Although formally estimated uncertainties are not available for either of these rotations, they nonetheless provide useful information about the overall scatter in the velocities

predicted by Pacific–North America rotations for times younger than 10.9 Ma. At 19.0°N, 105.5°W, the rotations for anomalies 4n.2 (7.90 Ma) and 3n.4 (5.12 Ma) predict respective velocities of 53.5 mm/yr toward N60°W and 59.3 mm/yr toward N59°W. The scatter in the rates predicted by these two rotations is thus the same as the 54–58 mm yr<sup>-1</sup> range of rates predicted by the 0.0, 3.16, and 10.9 Ma rotations. No clear pattern of acceleration, deceleration, or a change in the plate slip direction emerges. Although we cannot exclude the possibility that the 10% differences in the velocities averaged over these different times reflect actual changes in Pacific–North America motion since 10.9 Ma, we assume hereafter that the observed changes reflect the underlying level of noise.

In light of the evidence for relatively steady Pacific–North America velocities in the vicinity of the Rivera plate since  $\sim 10$  Ma, we opted to interpolate between the anomaly 2A.2 and anomaly 5n.2 rotations using two different sets of assumptions, corresponding to a minimum change model and a maximum change model. The minimum change model divides Pacific–North America motion since 10.9 Ma into two stages, one from the present to 3.16 Ma (anomaly 2A.2) and the other from 3.16 to 10.9 Ma. The stage rates during each interval are constant and average 54 and 60 mm/yr respectively, as required to yield the predicted 10.9 Ma-average rate of 58.3 mm/yr. This model prescribes the smallest possible difference in the stage spreading rates during the two intervals that will still yield the appropriate 10.9 Ma-average rate. Our maximum change model is also a two-stage model, but we instead assume that motion changed suddenly at 7.90 Ma (anomaly 4n.2), in accord with a change in the Pacific–North America direction at ca 7.9 Ma described by Atwater and Stock (1998). In this model, the stage rate is 54 mm/yr from 7.9 Ma to the present, but increases to 70 mm/yr from 10.9 to 7.9 Ma, once again yielding the required 10.9 Ma-average rate of 58.3 mm/yr. These two models are useful end-members amongst the many possible models that allow for either gradual or sudden changes in motion.

To construct rotations consistent with our mini-

imum change model, we used the Pacific–North America 2A.2 and 5n.2o rotations to derive the 2A.2–5n.2o stage rotation. We then interpolated the 2A.2–5n.2o stage rotation angle for ages intermediate between 3.16 and 10.9 Ma and summed the interpolated stage rotation to the anomaly 2A.2 finite rotation. For the maximum change model, we extrapolated the anomaly 2A.2 rotation to enforce constant Pacific–North America motion out to 7.9 Ma. We then solved for the 10.9–7.9 Ma stage rotation, interpolated this stage rotation to times between 7.9 and 10.9 Ma, and added the extrapolated stage rotations to the 7.9 Ma finite rotation.

To estimate uncertainties for times since 3.6 Ma, we used the 3.16 Ma rotation covariances to construct covariance matrices that yield  $1\sigma$  uncertainties of  $\pm 1$  mm/yr and  $\pm 1^\circ$ , which are appropriate for locations near the Rivera plate (DeMets and Dixon, 1999). For times older than 3.16 Ma, the uncertainties are known only for anomaly 5n.2 and thus must be either estimated or assigned values of zero. We chose to use the covariances for anomalies 2A.2 and 5n.2o to estimate uncertainties for our minimum and maximum change models. For the minimum change model, we used the covariances for the anomaly 2A.2 and 5n.2o finite rotations to solve rigorously for the 3.16–10.95 Ma stage rotation covariances and then scaled the stage covariances to intermediate times. For example, to solve for the covariances for the 3.16–5.12 Ma stage rotation, we multiplied each component of the  $3 \times 3$  covariance matrix for the 3.16 Ma–10.9 Ma stage rotation by a factor of  $(5.12-3.16)^2/(10.95-3.16)^2$ . For the maximum change model, we extrapolated the covariances for the anomaly 2A.2 finite rotation out to 7.9 Ma (by multiplying those covariances by a factor of  $7.90^2/3.16^2$ ). Using these, we solved for the 10.95–7.9 Ma stage rotation covariances and interpolated these covariances for intermediate age stage rotations following the procedure described above. We emphasize that uncertainties for all times intermediate between anomaly 5n.2 and anomaly 2A.2 are not propagated from anomaly and fracture zone crossings for those ages and may underestimate the true uncertainties.

### 5.6. Rivera–North America motion

Our reconstructions of displacement paths for points on the Rivera plate relative to North America and stage rates derived from Rivera–North America stage rotations (Fig. 11) change little if we employ our minimum-change or maximum-change model for Pacific–North America motion. This indicates that Rivera–North America motion since 9.9 Ma is influenced significantly more by changes in Pacific–Rivera motion than by the relatively small (10%) apparent changes in Pacific–North America motion. If the minimum-change and maximum-change models bracket the actual variations in Pacific–North America motion since 10.9 Ma, the differences in the Rivera–North America stage rates and displacement paths for the two models (Fig. 11) represent the approximate level of uncertainty introduced into estimates of Rivera–North America motion by uncertainties in Pacific–North America motion. The ensuing discussion thus applies for both of the two Rivera–North America models that we derived (Table 5).

Prior to 7.9 Ma, convergence of the Rivera plate with North America was approximately orthogonal to the trench along the southern part of the plate boundary (Fig. 11). The decrease in Rivera–North America convergence from rates of  $\sim 50$  mm/yr at 10–9 Ma to  $\sim 10$  mm/yr from  $\sim 8$  to 5 Ma is a kinematic consequence of changes in Pacific–Rivera motion from 10 to 5 Ma (Fig. 8). Our model predicts that Pacific–Rivera stage rates along the northern Middle America trench (Fig. 10) decreased by  $\sim 50\%$  from 10 to 5 Ma, far exceeding the uncertainties. By inference, the slowdown in Rivera–North America motion is highly significant, provided that Pacific–North America stage rates from 10 to 5 Ma behaved approximately as we assume (Fig. 10).

From 4.6 to 3.6 Ma, Rivera–North America convergence rates increased significantly everywhere along the plate boundary, and the motion of the Rivera plate was highly oblique to the plate boundary north of  $20^\circ\text{N}$  (Fig. 11). Given our assumption that Pacific–North America motion was constant during this interval and that observed Pacific–Rivera velocities at the paleo-rise axis (Fig. 8) also changed little or not at all, the

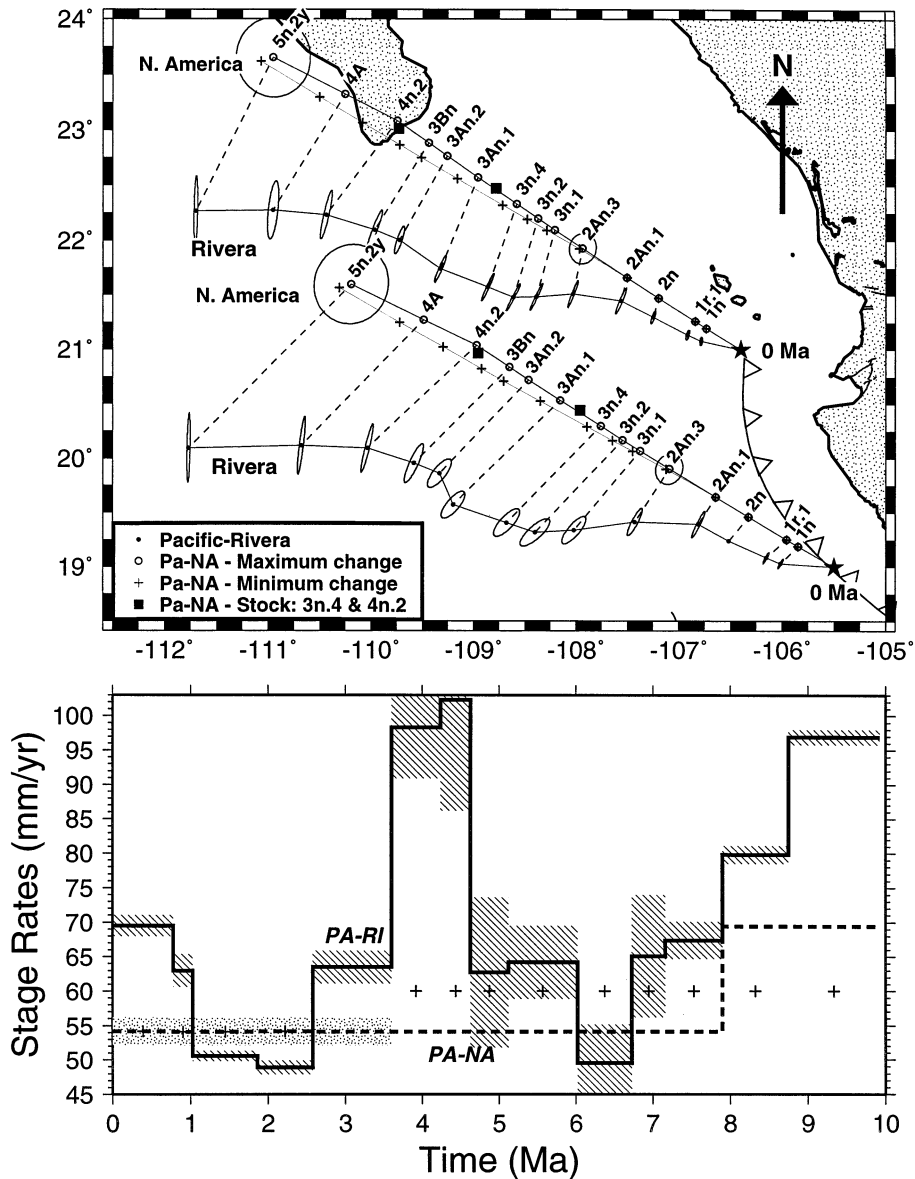


Fig. 10. Upper panel: reconstructed paths of the Rivera and North American plates for points along the present Rivera–North America plate boundary relative to the Pacific plate. Paths are constructed using Pacific–Rivera finite rotations (Tables 2 and 3) and Pacific–North America rotations are constructed using the minimum change and maximum change models described in text. Crosses and open circles show the paths predicted by the minimum change and maximum change models, respectively. Dashed lines connect reconstructed points of equal ages and thus show the relative finite displacements of points traveling with the Rivera and North American plates in a fixed Pacific plate reference frame. Squares show the reconstructed locations for anomalies 3n.4 and 4n.2 using rotations from J. Stock (pers. commun., 1999) and are included to help illustrate the level of uncertainty in the reconstructions. Error ellipses are 2-D 95%. Dark areas denote locations of Quaternary volcanism. Lower panel: Rivera and North America displacement rates (relative to the Pacific plate) along the reconstructed paths shown in the upper panel. Crosses show Pacific–North America stage rates predicted by the minimum change model; the dashed line shows stage rates predicted by the maximum change model. The shaded region depicts the  $1\sigma$  uncertainty. Uncertainties in stage rates do not incorporate uncertainties in magnetic reversal ages (see text). Uncertainties in Pacific–North America rates for times older than 3.6 Ma are poorly known and are not shown.

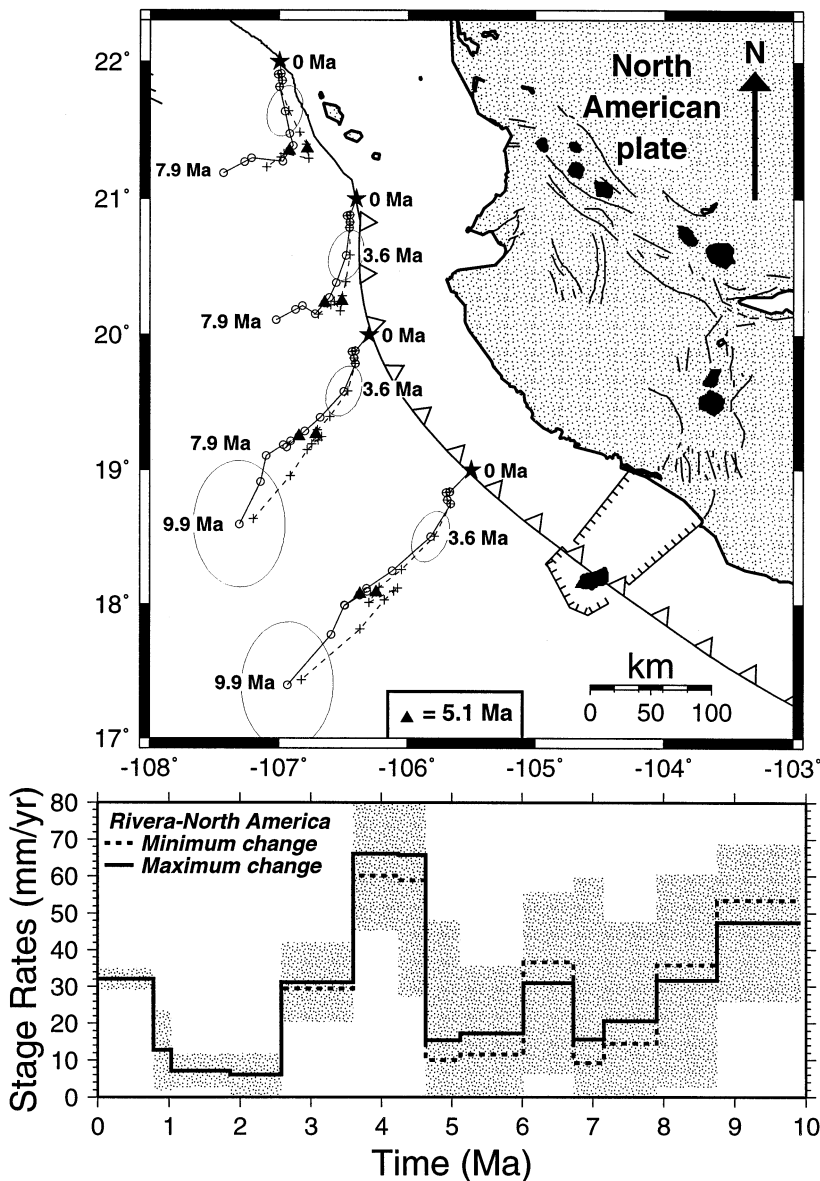


Fig. 11. Upper panel: reconstructed path of the Rivera plate relative to North America using Rivera–North America finite rotations (Table 5). Reconstructions based on the minimum change and maximum change models described in the text are shown respectively with crosses and open circles. Error ellipses are 2-D 95%. Solid triangles show reconstructed locations of anomaly 3n.4 (5.12 Ma) for the minimum and maximum change models. Lower panel: displacement rates along the flow line originating at 19°N for the minimum change and maximum change models. We assume that the Tres Marias escarpment (TME in Fig. 1) did not begin to accommodate Rivera–North America motion until at least 8 Ma. Points north of 21°N along the present plate boundary are thus not reconstructed for times older than 7.9 Ma. Uncertainties are  $1\sigma$ , but do not include uncertainties in magnetic reversal ages.

increase in Rivera–North America convergence rates may seem surprising. However, this is a geometric consequence of the apparent northeast-

ward migration of the Pacific–Rivera finite rotation pole from 4.6 to 3.6 Ma (anomaly 3n.2 to anomaly 2A.3). This migration altered the Pacific–

Rivera slip direction for points near the northern Middle America trench (Fig. 10) in a sense that increased Rivera–North America convergence. Southwestward migration of the Rivera–North America stage poles during this time changed the Rivera–North America direction by  $90^\circ$  CCW along the Middle America trench north of  $20^\circ\text{N}$  (Fig. 11). This imposed significant dextral shear north of  $20^\circ\text{N}$  and presumably shut off any subduction that was occurring if the Rivera plate shared a boundary with North America in this region prior to 5 Ma.

After  $\sim 3$  Ma, a profound change in Rivera–North America motion occurred (Fig. 11), associated with the significant decrease in Pacific–Rivera spreading rates that accompanied the major reorganization of the Rivera plate boundaries after 3.6 Ma (Fig. 9e–g). Rivera–North America motion slowed to  $6 \pm 8$  mm/yr (95% uncertainty) for a period of nearly two million years and rotated to a direction parallel to the trench (Fig. 11). The convergent component of motion between the two plates thus ceased entirely during this period, and motion, if there was any, consisted of boundary-parallel dextral shear everywhere along the trench. The cessation of subduction is a kinematic outcome of two changes in Pacific–Rivera motion after 3.6 Ma, one being a decrease in Pacific–Rivera stage rates to levels nearly identical to Pacific–North America stage rates for that period (Fig. 10) and the other being a shift in the location of the Pacific–Rivera pole (Fig. 6) that altered the Pacific–Rivera direction along the Middle America trench to a direction parallel with the Pacific–North America direction (Fig. 10).

A cessation or near-cessation of trench-normal convergence from 2.6–1.0 Ma seems likely to have occurred, subject to the reasonable assumption that the Jalisco block moved as part of the North American plate (or approximately so) during this period. Others have independently noted the decrease in Pacific–Rivera seafloor spreading rates during this period (Lonsdale, 1989; DeMets and Stein, 1990; Bandy, 1992), although none connected this slowdown to a cessation of Rivera–North America convergence. Moreover, the Pacific–Rivera rotations for times since 3.6 Ma are based on numerous unambiguous magnetic anom-

ally crossings with well-understood uncertainties. Similarly, estimates of Pacific–North America velocities for periods since 3.6 Ma from numerous geologic and geodetic data as well as global plate circuit closures are consistently  $48$ – $56$  mm/yr toward  $\text{N}60^\circ\text{W} \pm 3^\circ$  (DeMets et al., 1987; DeMets, 1995; DeMets and Dixon, 1999). Any of these velocities, particularly those with rates slower than the 54 mm/yr rate that we adopt, result in slow or zero Rivera–North America motion during this period.

After  $\sim 1.0$  Ma, Rivera–North America convergence resumed at a rate, and in a direction, remarkably close to those for 3.6–2.6 Ma (Fig. 11). The resumption of convergence coincided with a significant increase in Pacific–Rivera spreading rates and a CW rotation of the Pacific–Rivera direction (Figs. 9 and 10). Present-day (0–0.78 Ma) Rivera–North America motion consists of trench-normal convergence near the Manzanillo trough ( $18^\circ\text{N}$ ) at a rate of  $38 \pm 4$  mm/yr ( $2\sigma$ ) and increasingly oblique convergence at slower rates farther northwest along the trench (DeMets and Wilson, 1997). Three  $M=8$  shallow thrust earthquakes this century along the Rivera subduction zone (Singh et al., 1985; Escobedo et al., 1998) show that convergence still occurs.

### 5.7. Absolute motions of the Rivera and North American plates

To better understand the dynamics of Rivera plate motion, we also estimated its motion and that of the North American plate relative to the underlying mantle. To do this, we assumed that the hotspots are fixed in the mantle, and we combined Pacific–hotspot rotations with rotations for Pacific–North America and Pacific–Rivera motion. Unfortunately, the predictions of published models for Pacific–hotspot motion differ considerably. The HS2-NUVEL1 model predicts Pacific plate motion at Hawaii of 95 mm/yr toward  $\text{N}60^\circ\text{W}$  since 3 Ma (Gripp and Gordon, 1990). In contrast, a recently published model that assumes that the absolute motion of the Pacific plate changed significantly at 3 Ma predicts motion at Hawaii of 123 mm/yr toward  $\text{N}40^\circ\text{W}$  (Wessel and Kroenke, 1997). The evidence for a recent change

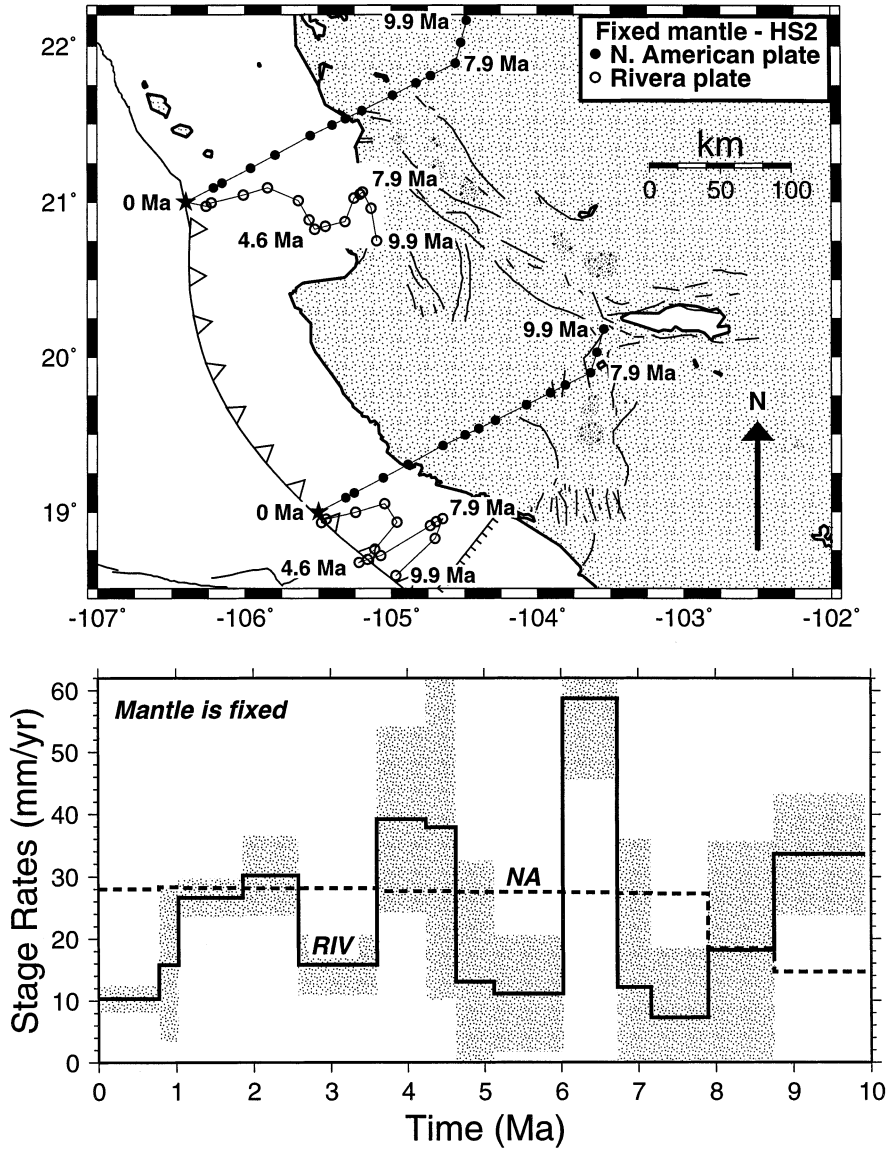


Fig. 12. Upper panel: reconstructed paths for points on the Rivera and North American plates relative to the underlying mantle. Pacific-hotspot rotations are described in text. The Pacific-North America rotations used to tie North America to the absolute reference frame correspond to our maximum-change model. Lower panel: displacement rates for the Rivera and North American plates relative to the underlying mantle for the flow line that originates at 19°N in the upper panel. Uncertainties are propagated solely from Pacific-Rivera rotation covariances and are thus minimum estimates.

in the Pacific plate’s absolute motion is based largely on the departure of the present Hawaiian hotspot location from the linear track defined by Hawaiian seamounts older than 3 Ma. This departure barely exceeds the underlying level of scatter

in seamount locations along the Hawaii-Emperor chain and in our view does not yet compel the conclusion that a recent change in the Pacific plate’s absolute motion has occurred.

To further assess the relative merits of these

two models, we used them to solve for the absolute motion of the North American plate at the Yellowstone hotspot. When combined with our 3.16 Ma Pacific–North America rotation, the HS2-NUVEL1 model yields a rotation for the absolute motion of North America that predicts motion of 21 mm/yr toward S53°W at the Yellowstone hotspot. This agrees well with age progressions of silicic volcanism and normal faulting along the Yellowstone hotspot track, which give an absolute North American plate velocity at Yellowstone of 15–30 mm/yr toward S52°W since 8 Ma (Smith and Braille, 1994). In contrast, the North American plate velocity predicted by the model based on the Wessel and Kroenke (1997) Pacific plate absolute rotation is 44 mm/yr toward S69°W, significantly faster than, and CW from, the observed velocity at Yellowstone.

We thus extrapolate the  $\sim 3$  Myr-average HS2-NUVEL1 Pacific plate rotation to describe Pacific plate absolute motion for all times since 10 Ma, and use the resulting rotations to solve for the absolute velocities of the Rivera and North American plates. Relative to the uncertainties in the relative plate velocities, the uncertainties in the mantle-fixed velocities are considerably larger and more difficult to quantify due to difficulties in estimating hotspot trends and propagation rates over periods of only a few Myr. In view of the poorly known uncertainties and our assumption that Pacific plate absolute motion has remained constant since 10 Ma, our estimate of Rivera plate motion relative to the mantle could be substantially in error.

Because we model Pacific–hotspot motion since 10 Ma as constant, the displacement history of the Rivera plate relative to the mantle (Fig. 12) reflects variations in Pacific–Rivera motion since 10 Ma. Our model predicts that the Rivera plate has alternated between eastward and westward motion along the southern, subduction-dominated part of the plate boundary. The predicted displacement of the Rivera plate relative to the mantle along this part of the plate boundary has been 70 km to the northwest, parallel to the present trench axis. Unlike most subducting plates, the Rivera plate thus does not move toward its subducting edges. Along the northern, shear-dominated part of the

plate boundary, the Rivera plate has moved  $\sim 120$  km westward (toward the plate boundary) since 10 Ma.

Since 7.9 Ma, the North American plate has moved west-southwest by  $\sim 200$  km at rates of  $\sim 30$  mm/yr relative to the mantle beneath western Mexico (Fig. 12). Assuming that Pacific–hotspot motion has been approximately constant since 10 Ma, North America has thus been steadily overriding the northern Middle America trench. In other regions where the overlying plate moves toward the subduction zone, neutral or moderately compressional tectonics typically occur within the overlying plate (Jarrard, 1986). Analogously, the Jalisco block should show evidence for neutral or moderately compressional tectonics. Although there is some evidence for significant uplift of the Jalisco region since  $\sim 4$  Ma (Richter et al., 1995), ample evidence for extension and associated volcanism within margin-parallel grabens argues against compressional tectonics in Jalisco since 10 Ma (Lange and Carmichael, 1991). Resolving this contradiction would require (at the very least) knowledge of the uncertainties in the hotspot rotations that is not available at present.

## 6. Discussion and summary

Our new model for Rivera–North America kinematics has several interesting implications for the tectonic evolution of the Jalisco region of western Mexico and the forces that drive motion of the Rivera plate. Following the lead of previous authors, we now speculate freely about some of those implications.

### 6.1. *Effects of stalled subduction on the Jalisco region*

The cessation of convergent motion between the Rivera and North American plates from 2.6 to 1.0 Ma (Fig. 11) raises important questions about the fate of the subducted slab that existed beneath the Jalisco block at 2.6 Ma. We believe the subducted slab could have responded in any of three ways: (1) it could have remained sus-

pended in the upper mantle, firmly attached to the unsubducted Rivera plate; (2) it could have detached from the unsubducted Rivera plate and subducted; or (3) it could have sunk vertically while remaining attached to the Rivera plate.

If the slab stagnated in the upper mantle while remaining attached to the unsubducted Rivera plate, its motion relative to the overlying North American plate and Jalisco block would have been principally northwestward (Fig. 11). This could have induced arc-normal extension within Jalisco during this period, possibly in the vicinity of the Colima graben. The temperature of the stalled slab would have increased due to the higher ambient temperature of the surrounding mantle, thereby altering its  $P$ – $T$  path in the mantle; however, thermal modeling would be required to determine whether this could have significantly changed the petrology of volcanics in Jalisco during the  $\sim 2$  Myr period of stalled subduction.

If the subducted slab detached from updip portions of the plate and continued to move down-dip at the 15 mm/yr absolute rate of the Rivera plate just prior to 3.6 Ma (Fig. 12), a gap of more than 20 km would have been created within the subducted Rivera plate during the  $\sim 1.5$  Myr hiatus in subduction. Tomographic imaging of the subducted slab may resolve such a gap if it exists. Detachment of the slab from the updip part of the Rivera plate implies the existence of a negative buoyancy contrast between the subducted plate and surrounding mantle. The apparent landward (NE-directed) absolute motion of the Rivera plate prior to 3.6 Ma is indirect evidence that a negative buoyancy contrast (Fig. 12) existed prior to the cessation of subduction, although the poorly known uncertainties in our Pacific–hotspot rotations preclude us from stating this with any confidence. If the slab instead remained attached to the Rivera plate but continued to sink vertically, the dip of the subducted slab may then have increased gradually. Such an increase would presumably have shifted the volcanic arc closer to the trench. Since the sinking rate of the subducted Rivera slab is unknown, we cannot predict how much the dip angle increased or how far the volcanic arc might have moved toward the trench. Some observations are consistent with trenchward arc migration.

Volcan de Colima and its predecessor Nevado de Colima are located closer to the trench than other Mexican volcanos (Luhr, 1992) and moreover show a north-to-south age progression indicative of trenchward arc migration (Allan, 1986). Steepening of the slab dip during a period of slow or no subduction might also help to explain why the subducting Rivera plate now dips more steeply than the adjacent Cocos plate (Pardo and Suarez, 1993). Few other factors predict a difference in the dips of these two plates — the subducting portions of both plates are approximately the same age (10–12 Ma); both plates are presently subducting at comparable rates (38–51 mm/yr); and the absolute motion of the overlying plate (North America) is the same.

### 6.2. *Rivera–North America motion and Jalisco block tectonics*

Prior to 3.6 Ma, two principal changes in Rivera–North America motion may have significantly affected the onshore volcano-tectonic record. After 5 Ma, motion became increasingly oblique to the plate boundary north of  $20^\circ\text{N}$  (Fig. 11) and presumably imposed significant dextral shear tractions along this part of the plate boundary. Our model predicts that as much as 50–100 km of margin-parallel motion occurred after 5 Ma north of  $20^\circ\text{N}$  (Fig. 11). This slip had to have been accommodated via some combination of oblique slip along the subduction zone fault, strike-slip motion along offshore faults in the continental margin, and extension or strike-slip motion along onshore faults (Bandy, 1992; Bandy and Pardo, 1994; Kostoglodov and Bandy, 1995). For example, abundant structural evidence and field relations indicates that faults along the Tepic–Zacoalco fault zone (Fig. 1) accommodated, and continue to accommodate, dextral slip (Ferrari et al., 1994; Moore et al., 1994; Richter et al., 1995). Alkaline volcanic rocks, frequently associated with continental rifting, first appear in the Colima graben at 4.6 Ma (Allan, 1986) and may date the onset of rifting in at least the northern Colima graben. Our reconstructions predict a margin-parallel component of only  $10 \pm 10$  km of Rivera–North America motion in the vicinity of

the Colima graben since 5 Ma, concentrated entirely between 2.6 and 1.0 Ma (Fig. 11). Although this agrees well with estimates of no more than several km of total opening across the northern Colima graben since ~5 Ma (Allan, 1986), rifting appears to have initiated long before 2.6 Ma. An alternative explanation for opening of the Colima graben is slow southeastward motion of crust located southeast of the Colima graben in response to oblique subduction of the Cocos plate (DeMets and Stein, 1990).

### 6.3. *Rivera plate deformation: an analog to the Gorda deformation zone?*

The pattern of deformed magnetic lineations in the southern Rivera plate resembles that of the deformed magnetic lineations in the Gorda deformation zone east of the southernmost Juan de Fuca rise (Stoddard, 1987). Magnetic lineations in both regions bend significantly clockwise as they approach the southern, right-lateral transform boundary of each plate. This raises the question of whether deformation in the Gorda region represents a useful modern-day analog to the paleo-deformation recorded in the southern Rivera plate. The Gorda region is deforming because the southern Juan de Fuca plate converges obliquely along its southern boundary with the Pacific plate, the Mendocino fracture zone. Analogously, suturing of the Mathematician plate to the Pacific plate after 3.3 Ma required the formation of new plate boundary faults at the southern edge of the Rivera plate (Fig. 9f and g). If pre-existing faults such as the Clarion fracture zone were not already parallel to the Pacific–Rivera slip direction at 3.3 Ma, any convergent component of motion across that rapidly evolving plate boundary could have deformed the interior of the Rivera plate via distributed dextral shearing or flexural slip, in a manner analogous to what is presently occurring in the Gorda region. Although such a model does not explain how deformation bypassed anomalies 4n.2, 4A, and 5n.2 on the Rivera plate, which are undeformed to within 50 km of the eastern Rivera transform fault (Fig. 2), suitable arrangements of faults south of the Rivera plate during the formation of the Rivera transform fault could be invoked

to solve this problem. Delineation of fossil faults preserved north and south of the Rivera transform fault from swath mapping data is needed to limit the range of possible paleo-fault geometries.

### 6.4. *Rivera plate dynamics: an analog to other oceanic microplates?*

Our work also raises questions about the forces that drive Rivera plate motion. Lonsdale (1995) demonstrates that the present rotation pole for the Rivera plate relative to the mantle is located close to the plate, which is often the case for oceanic microplates whose motions are strongly affected by forces acting along their edges. If slab pull were the principal force driving Rivera plate motion, the post-10 Ma absolute motion of the Rivera plate should have been consistently toward the subduction zone. The Rivera plate has instead moved consistently away from the subduction zone north of 20°N, where shear dominates the long-term relative motion, and has moved erratically relative to the mantle along the southern, subduction-dominated part of the plate boundary (Fig. 12). The present Rivera–North America convergence rate along the southern Rivera subduction zone, 32 mm/yr (Fig. 11), only slightly exceeds the 28 mm/yr rate at which the North American plate is overriding the subduction zone (Fig. 12). Convergence between these two plates is thus largely caused by seaward motion of the North American plate. These suggest that forces other than slab pull strongly influence Rivera plate absolute motion and possibly even dominate the force balance. This reinforces the idea that slab pull is not so important for young, and thus hot, oceanic plates.

If slab pull contributes little to the forces that drive Rivera plate motion, other forces must have ended the subduction hiatus from 2.6–1.0 Ma. We doubt that a ‘push’ from faster seafloor spreading after 1.0 Ma was responsible because there is little evidence that ridge push is a key plate driving force (Forsyth and Uyeda, 1975). We suspect instead that convergence resumed in response to decreased resistance to shear along the southern boundary of the Rivera plate once shear became concentrated along the present Rivera transform

fault. This interpretation is somewhat problematic because the Rivera transform fault was formed by 1.9 Ma, approximately 900 000 yr before subduction resumed. The onset of extension at or before 1.5 Ma across rupture zones in the northern Rivera plate (Lonsdale, 1995) might also explain the resurgence of subduction. These rupture zones partially decoupled the Rivera plate from its northernmost lithosphere, which shares a long shear boundary with North America that presumably acted to impede Rivera plate motion (Fig. 1).

As suggested by Stock and Lee (1994), the Rivera plate offers a useful modern analog to the oceanic microplates located west of Alta and Baja California that broke away from the Farallon plate and were captured by the Pacific plate between 30 and 12 Ma (Lonsdale, 1991). The progressive capture of the Monterey, Arguello, Guadelupe, and Magdalena microplates presumably reflects a larger-scale pattern of a loss of slab pull and stagnation of subduction as the spreading centers along the west flanks of these young oceanic plates approached the trench (Stock and Lee, 1994; Bohannon and Parsons, 1995). The Rivera plate exhibits similar behavior. Its lack of trenchward motion relative to the mantle since 10 Ma (Fig. 12) suggests that the net torque exerted by slab pull along the ~300 km where the Rivera plate subducts is small or is instead counterbalanced by the torques exerted by resistive forces acting on the plate.

If the Rivera plate ceases to exist as an independently moving microplate, it is unclear whether it will accrete to the Pacific plate, as did the now-extinct microplates west of California, or to North America. Motion of the Rivera plate relative to North America effectively stopped from 2.6 to 1.0 Myr (Fig. 11), and at least part of the plate now appears to move with the North American plate (Lonsdale, 1995; DeMets and Wilson, 1997). Although these could conceivably signal the eventual capture of the Rivera plate by North America, some kinematic evidence suggests that the Monterey and Arguello microplates moved with the North American plate prior to their capture by the Pacific plate (Atwater, 1989; Bohannon and Parsons, 1995). Ultimately, which of these two scenarios will occur, if either, will

depend on which one requires the least expenditure of energy. Suturing the Rivera plate to North America would require a cessation of subduction along the northern Middle America trench, realignment of the eastern 150 km of the Rivera transform fault to accommodate Pacific–North America slip, and little else, given that the western half of the Rivera transform fault is already nearly optimally aligned with the present Pacific–North America direction (Michaud et al., 1997). Suture of the Rivera plate to the Pacific plate would require southeastward propagation of the Gulf of California transform fault system to a point onshore from the northern end of the Pacific–Cocos rise, as well as extension in the vicinity of the Colima graben. The Tepic–Zacoalco fault zone and Colima graben are nearly optimally located for accommodating this transfer, which raises the question of whether they are evidence for an ongoing, or possibly aborted, transfer of the Rivera plate and Jalisco block to the Pacific plate.

### Acknowledgements

Ian Carmichael's enthusiasm for the volcanic rocks of the Jalisco region and their connection to the subducting Rivera plate was an important motivation for undertaking this work. We thank Tanya Atwater, Donna Jurdy, Kim Klitgord, Joann Stock, and Doug Wilson for thoughtful reviews that greatly improved this paper. We thank Steve Cande for providing the interactive software for picking anomaly crossings and Ted Chang for providing computer code for solving for best-fitting rotations. Figures were produced using Generic Mapping Tools software (Wessel and Smith, 1991). Support for this work was provided by NSF EAR-9205083, EAR-9526419, and the University of Wisconsin Alumni Research Foundation.

### References

- Allan, J.F., 1986. Geology of the northern Colima and Zacoalco grabens, southwest Mexico: late Cenozoic rifting in the Mexican volcanic belt. *Geol. Soc. Am. Bull.* 97, 473–485.

- Atwater, T., 1970. Implications of plate tectonics for the Cenozoic tectonic evolution of western North America. *Geol. Soc. Am. Bull.* 81, 3513–3536.
- Atwater, T., 1989. Plate tectonic history of the Northeast Pacific and Western North America. In: Winterer, E.L., Hussong, D.M., Decker, R.W. (Eds.), *The Eastern Pacific Ocean and Hawaii — The Geology of North America N*. Geological Society of America, Boulder, pp. 21–72.
- Atwater, T., Stock, J., 1998. Pacific–North America plate tectonics of the Neogene Southwestern United States: An update. *Int. Geol. Rev.* 40, 375–402.
- Bandy, W.L., 1992. Geological and geophysical investigation of the Rivera-Cocos plate boundary: Implications for plate fragmentation. Ph.D. thesis, Texas A&M University, College Station, TX.
- Bandy, W., Pardo, M., 1994. Statistical examination of the existence and relative motion of the Jalisco and southern Mexico blocks. *Tectonics* 13, 755–768.
- Bandy, W., Mortera-Gutierrez, C., Urrutia-Fucugauchi, J., Hilde, T.W.C., 1995. The subducted Rivera-Cocos plate boundary: Where is it, what is it, and what is its relationship to the Colima rift? *Geophys. Res. Lett.* 22, 3075–3078.
- Bandy, W.L., Kostoglodov, V.V., Mortera-Gutierrez, C.A., Urrutia-Fucugauchi, J., 1998. Comment on ‘Relative motions of the Pacific, Rivera, North American, and Cocos plates since 0.78 Ma’ by Charles DeMets and Douglas S. Wilson. *J. Geophys. Res.* 103, 24 245–24 250.
- Bohannon, R.G., Parsons, T., 1995. Tectonic implications of post-30 Ma Pacific and North American relative plate motions. *Geol. Soc. Am. Bull.* 107, 937–959.
- Bourgeois, J., Renard, V., Aubouin, J., et al., 1988. Fragmentation en cours du bord Ouest du Continent Nord Américain: Les frontieres sous-marines du Bloc Jalisco (Mexique). *C. R. Acad. Sci. Paris* 307, 1121–1130.
- Cande, S.C., Kent, D.V., 1995. Revised calibration of the geomagnetic polarity timescale for the Late Cretaceous and Cenozoic. *J. Geophys. Res.* 100, 6093–6095.
- Chang, T., 1988. Estimating the relative rotation of two tectonic plates from boundary crossings. *J. Am. Stat. Assoc.* 83, 1178–1183.
- Chang, T., Stock, J., Molnar, P., 1990. The rotation group in plate tectonics and the representation of uncertainties of plate reconstructions. *Geophys. J. Int.* 101, 649–661.
- Delgado Granados, H., 1993. Late Cenozoic tectonics offshore western Mexico and its relation to the structure and volcanic activity in the western Trans-Mexican Volcanic Belt. *Geofis. Int.* 32, 543–559.
- DeMets, C., Gordon, R.G., Stein, S., Argus, D.F., 1987. A revised estimate of Pacific–North America motion and implications for western North America plate boundary zone tectonics. *Geophys. Res. Lett.* 14, 911–914.
- DeMets, C., Stein, S., 1990. Present-day kinematics of the Rivera plate and implications for tectonics of southwestern Mexico. *J. Geophys. Res.* 95, 21 931–21 948.
- DeMets, C., 1995. A reappraisal of seafloor spreading lineations in the Gulf of California: Implications for the transfer of Baja California to the Pacific plate and estimates of Pacific–North America motion. *Geophys. Res. Lett.* 22, 3545–3548.
- DeMets, C., Wilson, D.S., 1997. Relative motions of the Pacific, Rivera, North American, and Cocos plates since 0.78 Ma. *J. Geophys. Res.* 102, 2789–2806.
- DeMets, C., Dixon, T., 1999. New kinematic models for Pacific–North America motion from 3 Ma to present: Evidence for steady motion and biases in the NUVEL-1A model. *Geophys. Res. Lett.* 26, 1921–1924.
- Engebretson, D.C., Cox, A., Gordon, R.G., 1985. Relative motions between oceanic and continental plates in the Pacific basin. *Geol. Soc. Am. Spec. Pap.* 206, 59 pp.
- Escobedo, D., Pacheco, J.F., Suárez, G., 1998. Teleseismic body-wave analysis of the 9 October, 1995 ( $M_w=8.0$ ), Colima-Jalisco, Mexico earthquake and its largest foreshock and aftershock. *Geophys. Res. Lett.* 25, 547–550.
- Fernandez, L.S., Hey, R.N., 1991. Late Tertiary tectonic evolution of the seafloor spreading system off the coast of California between the Mendocino and Murray fracture zones. *J. Geophys. Res.* 96, 17 955–17 979.
- Ferrari, L., Pasquarè, G., Venegas, S., Castillo, D., Romero, F., 1994. Regional tectonics of western Mexico and its implications for the northern boundary of the Jalisco block. *Geofis. Int.* 33, 139–151.
- Forsyth, D.W., Uyeda, S., 1975. On the relative importance of the driving forces of plate motion. *Geophys. J. R. Astron. Soc.* 43, 163–200.
- Gripp, A.E., Gordon, R.G., 1990. Current plate velocities relative to the hotspots incorporating the NUVEL-1 global plate motion model. *Geophys. Res. Lett.* 17, 1109–1112.
- Hellinger, S.J., 1979. The statistics of finite rotations in plate tectonics. Ph.D. thesis, Massachusetts Institute of Technology, 172.
- Hellinger, S.J., 1981. The uncertainties of finite rotations in plate tectonics. *J. Geophys. Res.* 86, 9312–9318.
- Henry, C.D., Aranda-Gomez, J.J., 2000. Plate interactions control middle-late Miocene proto-Gulf and Basin and Range extension in the southern Basin and Range. *Tectonophysics* 318.
- Hilgen, F.J., Krijgsman, W., Langereis, C.G., Lourens, L.J., Santarelli, A., Zachariasse, W.J., 1995. Extending the astronomical (polarity) time scale into the Miocene. *Earth Planet. Sci. Lett.* 136, 495–510.
- Jarrard, R.D., 1986. Relations among subduction parameters. *Rev. Geophys.* 24, 217–284.
- Johnson, C.A., Harrison, C.G. A., 1990. Neotectonics in central Mexico. *Phys. Earth Planet. Inter.* 64, 187–210.
- Klitgord, K.D., Mammerickx, J., 1982. Northern East Pacific Rise: Magnetic anomaly and bathymetric framework. *J. Geophys. Res.* 87, 6725–6750.
- Kostoglodov, V., Bandy, W., 1995. Seismotectonic constraints on the rate between the Rivera and North American plates. *J. Geophys. Res.* 100, 17 977–17 990.
- Lange, R.A., Carmichael, I.S.E., 1991. A potassic volcanic front in western Mexico: The lamprophyric and related lavas of San Sebastian. *Geol. Soc. Am. Bull.* 103, 928–940.
- Lipman, P.W., 1980. NRC Geophysics Study Committee

- (Eds.), *Cenozoic Volcanism in the Western United States: Implications for Continental Tectonics*. National Research Council, Washington, DC, pp. 161–174.
- Lonsdale, P., 1989. Geology and tectonic history of the Gulf of California. In: Winterer, E.L., Hussong, D.M., Decker, R.W. (Eds.), *The Eastern Pacific Ocean and Hawaii: The Geology of North America N*. Geological Society of America, Boulder, CO, pp. 499–521.
- Lonsdale, P., 1991. Structural patterns of the Pacific floor offshore of Peninsular California. In: Dauphin, J.P., Simoneit, B.R.T. (Eds.), *Gulf and Peninsular Provinces of the Californias*, Am. Assoc. Pet. Geol. Mem. 47, 87–125.
- Lonsdale, P., 1995. Segmentation and disruption of the East Pacific rise in the mouth of the Gulf of California. *Mar. Geophys. Res.* 17, 323–359.
- Luhr, J.F., Nelson, S.A., Allan, J.F., Carmichael, I.S.E., 1985. Active rifting in southwestern Mexico: Manifestations of an incipient eastward spreading-ridge jump. *Geology* 13, 54–57.
- Luhr, J.F., 1992. Slab-derived fluids and partial melting in subduction zones: Insights from two contrasting Mexican volcanoes (Colima and Ceboruco). *J. Volcanol. Geotherm. Res.* 54, 1–18.
- Macdonald, K.C., Scheirer, D.S., Carbotte, S.M., 1991. Mid-ocean ridges: Discontinuities, segments and giant cracks. *Science* 253, 986–994.
- Mammerickx, J., Naar, J.F., Tyce, R.L., 1988. The Mathematically paleoplate. *J. Geophys. Res.* 93, 3025–3040.
- Michaud, F., Royer, J.-Y., Bourgois, J., Mercier de Lepinay, B., Liaudon, G.P., 1997. The Rivera fracture zone revisited. *Mar. Geol.* 137, 207–225.
- Moore, G., Marone, C., Carmichael, I.S.E., Renne, P., 1994. Basaltic volcanism and extension near the intersection of the Sierra Madre volcanic province and the Mexican volcanic belt. *Geol. Soc. Am. Bull.* 106, 383–394.
- Nicholson, C., Sorlien, C., Atwater, T., Crowell, J., Luyendyk, B., 1994. Microplate capture, rotation of the Western Transverse Ranges, and initiation of the San Andreas Transform as a low-angle fault system. *Geology* 22, 491–495.
- Nieto-Samaniego, A.F., Ferrari, L., Alaniz-Alvarez, S.A., Labarthe-Hernandez, G., Rosas-Elguera, J., 1999. Variation of Cenozoic extension and volcanism across the southern Sierra Madre Occidental volcanic province, Mexico. *Geol. Soc. Am. Bull.* 111, 347–363.
- Nixon, G.T., 1982. The relationship between Quaternary volcanism in central Mexico and the seismicity and structure of subducted oceanic lithosphere. *Geol. Soc. Am. Bull.* 93, 514–523.
- Pardo, M., Suarez, G., 1993. Steep subduction geometry of the Rivera plate beneath the Jalisco block in western Mexico. *Geophys. Res. Lett.* 20, 2391–2394.
- Pasquarè, G., Garduño, V.H., Tibaldi, A., Ferrari, L., 1988. Stress pattern evolution in the central sector of the Mexican Volcanic Belt. *Tectonophysics* 146, 353–364.
- Righter, K., Carmichael, I.S.E., Becker, T.A., Renne, P.R., 1995. Pliocene–Quaternary volcanism and faulting at the intersection of the Gulf of California and the Mexican Volcanic Belt. *Geol. Soc. Am. Bull.* 107, 612–626.
- Royer, J.Y., Chang, T., 1991. Evidence for relative motions between the Indian and Australian plates during the last 20 Myr from plate tectonic reconstructions: Implications for the deformation of the Indo-Australian plate. *J. Geophys. Res.* 96, 11 779–11 802.
- Singh, S.K., Ponce, L., Nishenko, S.P., 1985. The great Jalisco, Mexico, earthquakes of 1932: Subduction of the Rivera plate. *Bull. Seismol. Soc. Am.* 75, 1301–1313.
- Smith, R.B., Braille, L.W., 1994. The Yellowstone hotspot. *J. Volcanol. Geotherm. Res.* 61, 121–187.
- Stein, S., Gordon, R.G., 1984. Statistical tests of additional plate boundaries from plate motion inversions. *Earth Planet. Sci. Lett.* 69, 401–412.
- Stock, J., Molnar, P., 1988. Uncertainties and implications of the Late Cretaceous and Tertiary position of North America relative to the Farallon, Kula, and Pacific plates. *Tectonics* 7, 1339–1384.
- Stock, J.M., Hodges, K.V., 1989. Pre-Pliocene extension around the Gulf of California and the transfer of Baja California to the Pacific plate. *Tectonics* 8, 99–115.
- Stock, J.M., Lee, J., 1994. Do microplates in subduction zones leave a geological record? *Tectonics* 13, 1472–1487.
- Stoddard, P.R., 1987. A kinematic model for the evolution of the Gorda plate. *J. Geophys. Res.* 92, 11 524–11 532.
- Wallace, P., Carmichael, I.S.E., Righter, K., Becker, T.A., 1992. Volcanism and tectonism in western Mexico: A contrast of style and substance. *Geology* 20, 625–628.
- Wessel, P., Smith, W.H.F., 1991. Free software helps map and display data. *EOS Trans. Am. Geophys. U.* 72, 441–446.
- Wessel, P., Kroenke, L., 1997. A geometric technique for relocating hotspots and refining absolute plate motions. *Nature* 387, 365–369.
- Wilson, D.S., 1993a. Confidence intervals for motion and deformation of the Juan de Fuca plate. *J. Geophys. Res.* 98, 16 053–16 071.
- Wilson, D.S., 1993b. Confirmation of the astronomical calibration of the magnetic polarity timescale from sea-floor spreading rates. *Nature* 364, 788–790.
- Wilson, D.S., DeMets, C., 1998. Reply to Comment on ‘Relative motions of the Pacific, Rivera, North American, and Cocos plates since 0.78 Ma’. *J. Geophys. Res.* 103, 24 251–24 256.